LASER INTERFEROMETER GRAVITATIONAL WAVE OBSERVATORY

LIGO Laboratory / LIGO Scientific Collaboration

LIGO-T0900304-v2 *LIGO* June 19, 2009

Advanced LIGO Thermal Compensation System Preliminary Design

Phil Willems, Aidan Brooks, Mike Smith, Ken Mailand

Distribution of this document:
LIGO Scientific Collaboration

This is an internal working note
of the LIGO Project.

California Institute of Technology
LIGO Project – MS 18-34
1200 E. California Blvd.
Pasadena, CA 91125
Phone (626) 395-2129
Fax (626) 304-9834
E-mail: info@ligo.caltech.edu

Massachusetts Institute of Technology
LIGO Project – NW22-295
185 Albany St
Cambridge, MA 02139
Phone (617) 253-4824
Fax (617) 253-7014
E-mail: info@ligo.mit.edu

LIGO Hanford Observatory
P.O. Box 1970
Mail Stop S9-02
Richland WA 99352
Phone 509-372-8106
Fax 509-372-8137

LIGO Livingston Observatory
P.O. Box 940
Livingston, LA 70754
Phone 225-686-3100
Fax 225-686-7189

http://www.ligo.caltech.edu/

1 Introduction and Scope

The Thermal Compensation System comprises several separate subsystems that collectively sense and correct thermal aberrations in the core optics of the interferometer, specifically: the Input Test Masses (ITMs), Compensation Plates (CPs), and End Test Masses (ETMs). Thermal aberrations in other core optics, such as the Beamsplitter (BS), Power Recycling Mirror (PRM) and Signal Recycling Mirror (SRM) are expected to be ignorably small. Thermal aberrations in the Prestabilized Laser (PSL) or Input Optics (IO) are expected to be significant but these lie within the scope of those subsystems.

The subsystems of TCS are: the Test Mass Shielded Ring Heater, the CO_2 Laser Projector, the ITM/CP Hartmann Sensor, the ETM Hartmann Sensor, the Bull's-eye Sensor, and the Phase Camera. The Optical Lever System (Oplev) will also contain some TCS functionality, but its design is outside the scope of this document.

2 Relevant Documents

"Auxiliary Optics Support System Conceptual Design Document, Vol. 1: Thermal Compensation System," LIGO Document T060083-01-D.

"Decision to Adopt Hartmann Sensors over WLISMI Sensors for Advanced LIGO TCS," Record of Decision/Agreement M070025-00-Y.

"Core Optics Components Preliminary Design," LIGO Document E080033-00-D.

"Auxiliary Optics Support System Design Requirements Document, Vol. 1: Thermal Compensation System," LIGO Document T000092-02-D.

"List of Items Used in and around the Test Mass," LIGO document T0900092-v5.pdf, and related documents.

"Active Wavefront Correction in Laser Interferometric Gravitational Wave Detectors," Ryan Lawrence, Ph.D. thesis, MIT (2003).

"Enhanced LIGO TCS Review," LIGO document T080004-00-D.

"Enhanced LIGO TCS CO_2 Laser Intensity Servo Requirements," LIGO document T070224-01-D.

"Low Noise Preamplifier," LIGO Document D070254.

"TCS ISS Servo Board," LIGO Document D080351.

"TCS AA Interface Board," LIGO Document D080315.

"TCS Actuator Noise Coupling," LIGO Document T060224-00-D.

"TCS Viewport Details," LIGO Document E080448-00-V.

"TCS ZnSe Viewport Protection Window Assembly," LIGO Document D080617-v1.

"Ultra-sensitive wavefront measurement using a Hartmann sensor," A. Brooks *et al.,* Optics Express 15 (2007), pp. 10370-5.

"Direct Measurement of Absorption-Induced Wavefront Distortion in High Optical Power Systems," A. Brooks *et al.,* Applied Optics 48 (2009) pp. 355-64.

"AdvLIGO Interferometer Sensing and Control Preliminary Design," LIGO Document T0900175-v1.

"Hartmann Wavefront Sensors for Advanced Gravitational Wave Interferometers," Aidan Brooks, Ph.D. thesis, University of Adelaide (2007).

"Input Optics Final Design," LIGO document LIGO T980009-01-D, section 9.3.

"Determination and Optimization of Mode Matching into Optical Cavities by Heterodyne Detection," G. Mueller *et al.,* Optics Letters 25 (2000), pp. 266-8.

"LIGO Interferometer Operating at Design Sensitivity with Application to Gravitational Radiometry," Stefan Ballmer, Ph.D. thesis, MIT (2006).

"Frequency Resolving Spatiotemporal Wavefront Sensor," K. Goda *et al.,* Optics Letters **29**, pp.1452-1454 (2004).

3 Significant Changes to TCS since the Conceptual Design

3.1 Change of Shielded Ring Heater Scope and Design

The Conceptual Design of Advanced LIGO TCS[1] considered a shielded ring heater similar to that tested by Ryan Lawrence at MIT as the primary means to apply corrective heating to the compensation plate. However, this design was incompatible with the quadruple suspension design, for three reasons.

1) The quadruple suspension does not provide sufficient optical access for the shielded ring heater to illuminate the CP from all necessary angles.
2) The shielded ring heater uses shields to tailor the spatial profile of the heating, which makes it inefficient. Assuming nondirectional radiance from the ring heater element, the heater must dissipate ~170W to deliver 6W to the CP. Safely dissipating this heat

[1] LIGO Document T060083-01-D.

away from the thermally sensitive quad suspension structure in close proximity would be very difficult.

3) There is no space for a shielded ring heater between the CP and the FM in the folded interferometer.

Since the CO_2 laser projector is already being designed to provide sufficient power to the CP, and with a more flexible spatial distribution, the design has been changed to allocate all heating of the CP to the CO_2 laser projector.

The ring heater now serves the role of controlling the radii of curvature of all four TM HR surfaces, by heating a band around the circumference of the mirrors near the AR face, and has been moved within the SUS quad structure for this purpose. This clearly produces a thermal lens in the ITM substrate, and one that provides some compensation of the thermal lens due to self-heating. The combined operation of the ring heater and CO_2 laser projector will be discussed in a later section.

3.2 Change of Carbon Dioxide Laser Projector Scope

As discussed in Section 3.1, the CO_2 laser projector now provides all the compensation heating to the CP.

3.3 Choice of the Hartmann Sensor as the ITM/CP and ETM Dedicated Sensor

The wedge angles and tilts of the ITM and CP do not permit any of the AR surfaces of either optic to produce the reference wavefront for the WLISMI sensor, as reflections from these surfaces take an entirely different optical path and are dumped. This makes the WLISMI technology impractical for use as the ITM/CP sensor in LIGO. For this reason, the Hartmann sensor, which also demonstrates adequate sensitivity, has been chosen.[2]

3.4 Choice of Modified Two-Beam Optical Lever as TM HR Surface Dedicated Sensor

The change in the TM HR radii of curvature, if not corrected by the shielded ring heaters as discussed in Section 3.1, will produce tilts on the mirror surface of order 1 microradian, which is the same level of tilt the optical levers are built to detect. The uncertainty in the optical lever is dominated by instability in the optical lever pier. Therefore a two-beam optical lever has been designed for the TM HR surface monitor. In this design, the pier drift is common to the two beams and the TM radius of curvature is differential to the two beams. This design is presented more fully in Section 4.4.

[2] Record of Decision/Agreement M070025-00Y.

3.5 Change in Number and Layout of Dedicated Sensors

3.5.1 No BS Hartmann Sensor

The BS in Advanced LIGO will use very low absorption Heraeus 3001 fused silica as its substrate material. Heraeus 3001 has 0.02 ppm/cm absorption,[3] as opposed to the 2 ppm/cm absorption assumed in the Design Requirements.[4] This reduces the BS contribution to the thermal lens from ~10% to ~0.1% of the contribution from the ITM/CP pair, making it negligible enough not to require separate monitoring.

3.5.2 ETM Transmission Hartmann Sensor

A Hartmann sensor will probe the ETM through its AR surface. Its purpose will be to provide a higher resolution monitor of the absorption on the ETM surface for diagnostic purposes.

3.5.3 Revised ITM/CP Hartmann Probe Beam Injection Paths

Since the Conceptual Design Review of Advanced LIGO, there have been several relevant changes to the Advanced LIGO baseline design. First is the adoption of stable recycling cavities, which will be done by incorporating the input and output mode-matching telescopes into the power and signal recycling cavities, respectively. Second, and related, are changes in the Core Optics positions and wedge angles. Third is the elimination of the large pickoff telescope for ISC sensing beams that the Hartmann sensors would have used. These have driven a review of the possibilities for injecting the Hartmann probe beams.

The new Hartmann probe beam injection/extraction scheme uses the signal cavity telescope mirrors SM2 and SM3 to magnify the beams, and injects/extracts the probe beams through or near SM2. This scheme is described in more detail in Sections 4.3.4.2 and 4.3.4.3.

4 TCS Subsystem Descriptions

4.1 Shielded Ring Heater

A shielded ring heater will surround each ITM and ETM, to provide a band of heating around the circumference of the mirror 40 mm away from its AR surface. The primary purpose of the shielded ring heater is to reduce the radius of curvature of the HR surface of its mirror, and thereby maintain the correct arm cavity mode structure. Both thermal deformation due to absorbed interferometer beam power and static curvature errors due to incorrect polish can be compensated in this way.

The thermal flexure of an Advanced LIGO mirror is very closely approximated by a spherical curvature at the HR face if the rear half of the mirror is heated axisymmetrically. Precisely how the heat is distributed is not very important, so long as it is axisymmetric.

Given the close proximity of the compensation plate or reaction mass to the rear face of the test mass, and of the suspension structure elsewhere, the most convenient location for the ring heater is

[3] "Core Optics Components Preliminary Design," LIGO document E080033-00-D.

[4] "Auxiliary Optics Support System Design Requirements Document, Vol. 1: Thermal Compensation System" LIGO document T000092-02-D.

mounted directly to the lower quad suspension structure, on the front face of the octagonal brace surrounding the rear part of the test mass. A cutaway drawing of the ring heater, and its installation in the quad SUS are given in Figure 1.

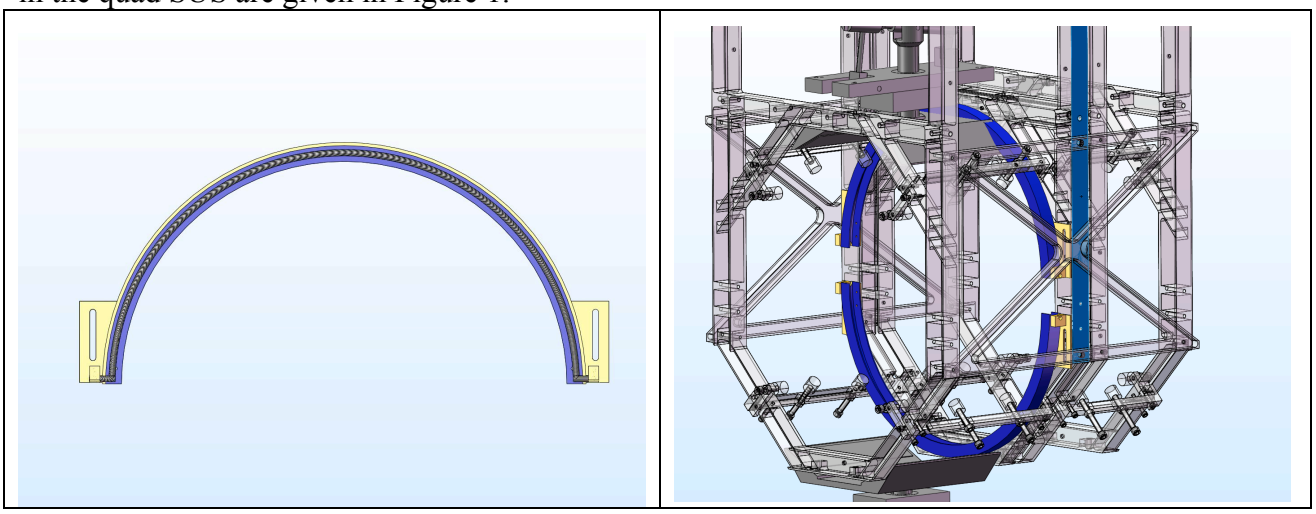

Figure 1: Left, upper ring heater cutaway view. Right, ring heater installed into quad SUS.

The heater itself is a coil of nichrome wire held upon a fused silica former. It has a total resistance of 100-1000 ohms, depending upon the wire gauge and number of turns around the former. Finite-element modeling shows that up to 20W of radiant power is needed to provide sufficient correction of the thermal ROC change in a test mass; the resistance range specified allows this power to be supplied to the ring heater by fairly ordinary power supplies of 50-140V, .15-.4A.

The assembly of the quadruple suspension requires that the ring heater be installed into the suspension structure before the test mass as two separate half-circles with a vertical gap between them, which can then be closed into a full circle after the suspension fibers are welded.[5]

The shielding of the ring heater has a gold inner coating. This reflects incandescent heat emitted from the coil outward from the test mass back to the test mass, using the coil power more efficiently. This allows the heater to run at lower temperature and protects the suspension structure from direct heating by the coil. The mechanical mounting of the ring heater to the shield is via the mounting blocks at the sides, which captivate the fused silica former rod in the 0.197" through holes when they are bolted to the rest of the shield. The smaller 0.079" though holes are pass-throughs for the nichrome wire- these are insulated with fused silica tubing glued into place with vacuum epoxy. The slots in the shield allow the ring heater to be moved up and down during the suspension assembly.

The cabling for the ring heater attaches to spade lugs crimped onto the nichrome wire ends after they are threaded through the mounting blocks. This cabling consists of three bundled 28AWG multistrand wires per heater end (two per half-circle, four in all) from Cooner Wire Company (part no. CZ1105) with crimped spade lugs at the ring heater ends and vacuum-compatible D-sub connectors for electrical coupling to outside the vacuum. The lengths of these cables will be determined by the distances to the electrical feedthroughs in the BSC chambers, which are not currently known, but should be roughly 6 meters as was used in the LASTI prototype. This cabling

[5] "List of Items Used in and around the Test Mass," LIGO document T0900092-v5.pdf, and related documents.

snakes up the suspension support structure and across the seismic isolation on its way to the feedthough. Attachment points for cable anchors are provided on the suspension support structures.

Any thermal compensator works by altering the phase profile of the optic, and so fluctuations in the compensation power can inject noise into the interferometer. The ring heater is no exception, even though it does not act on the test mass HR surface. Therefore, the power delivered to the ring heater must be quiet to some level.

The flexure of the test mass under thermoelastic expansion in a thin surface layer under the ring heater due to 1W fluctuations at 100 Hz were modeled in COMSOL. The motion of the center of the HR surface relative to the average motion of the whole mass in the model gave the injected noise motion to be 9.47×10^{-16} m. The noise requirement on TCS at 100 Hz must be less than 10^{-24} m/√Hz.[6] Although this requirement is overly strict and should be relaxed, for now it implies a TCS power noise of 10^{-9} W out of 11W delivered power, or a RIN of 10^{-10}/√Hz.

Such a noise level is impossible to measure, but should be simple to achieve, since the ring heater thermally averages fluctuations in the power delivered to it. The thermal time constant of the Advanced LIGO ring heater has not been measured, but that used by Ryan Lawrence is similar in construction, and had a measured time constant of 300 s.[7] At 100 Hz, the expected 1/f rolloff in output power fluctuations implies that the power supply to the ring heater needs an output power stability of only 3×10^{-6}/√Hz. The commissioning of the ring heater should include a measurement of the transfer function between supplied heater power and mirror surface displacement, and the supply power should be monitored with sufficient sensitivity to detect glitches capable of producing detectable signals at the IFO output port.

4.2 CO_2 Laser Projector

4.2.1 Overall Design Philosophy

Figure 2 shows the schematic layout of the CO_2 laser projector. This design contains elements from the Enhanced LIGO TCS projector and the Virgo TCS projector.

[6] "Auxiliary Optics Support System Design Requirements Document, Vol. 1: Thermal Compensation System" LIGO document T000092-02-D.

[7] "Active Wavefront Correction in Laser Interferometric Gravitational Wave Detectors," Ryan Lawrence, Ph.D. thesis, MIT (2003).

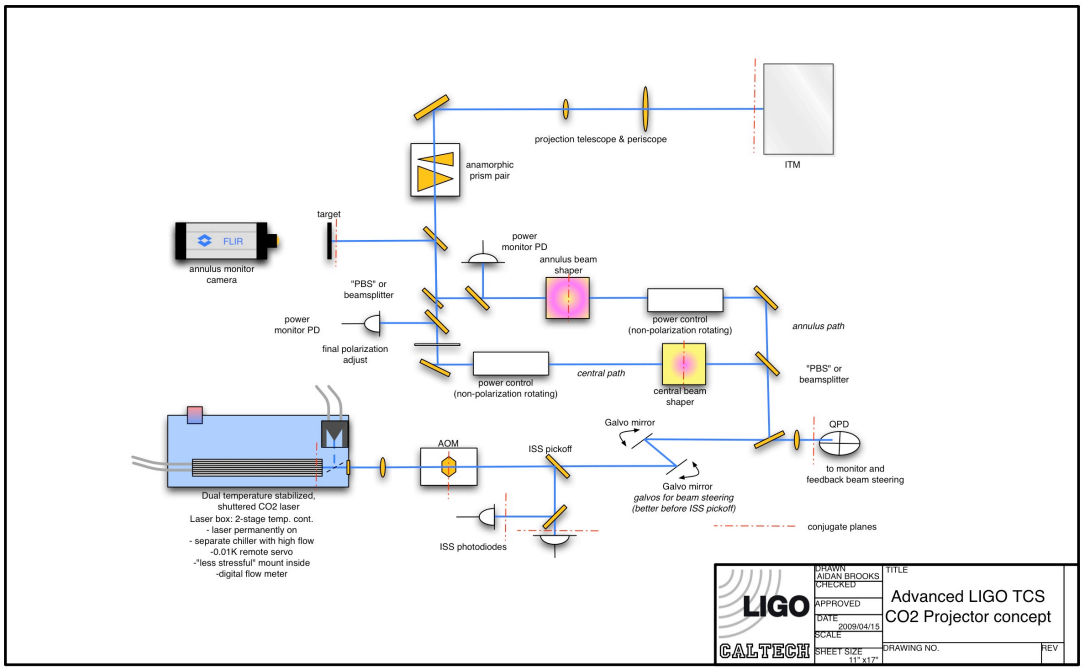

Figure 2: schematic layout of CO_2 laser projector.

The Enhanced LIGO TCS projector served not only to compensate Enhanced LIGO but also as a prototype of the Advanced LIGO design.[8] Numerous unforeseen difficulties were discovered in commissioning the projector, leading to several changes in its layout, with more to be made for Advanced LIGO. The originally proposed layout can be found in LIGO-G080004-00, and the current layout is given in Figure 3.

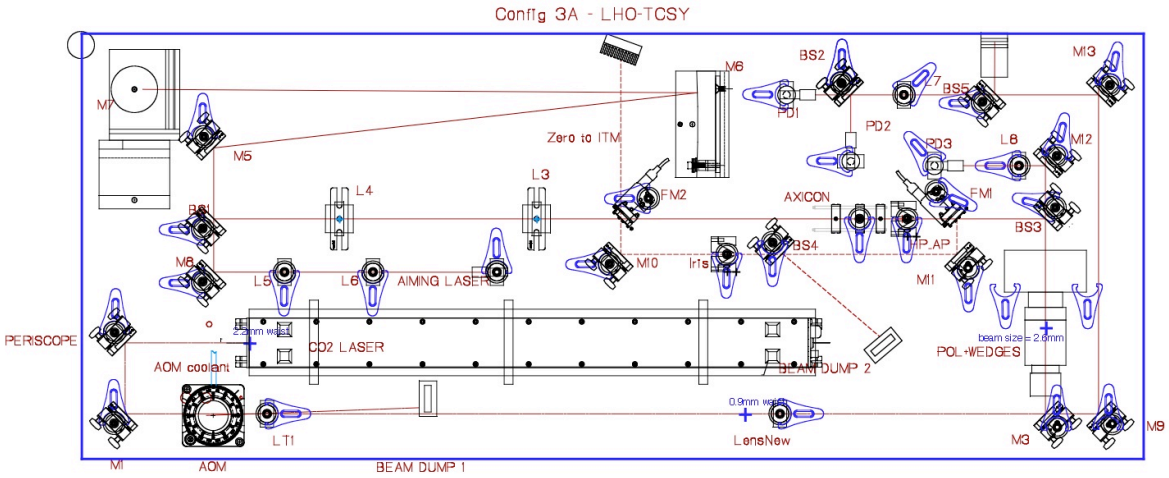

Figure 3: Enhanced LIGO TCS projector layout.

The Enhanced LIGO projectors exhibited slow distortions of the annular heat pattern and slow drift of the central and annular pattern pointing. Beam wander was generally the cause of these

[8] "Enhanced LIGO TCS Review," LIGO document T080004-00-D.

difficulties. Improvements to individual components in the projector resolved many of these problems, and these are discussed below in the descriptions of those components. The optical layout can be designed in such a way as to minimize the sensitivity of the delivered heating pattern to these drifts, by reimaging the aperture plane of any component that can deflect the beam to the aperture plane of the beam shaping optics, and then to the CP face. This was not practical within the constraints of the Enhanced LIGO projector, but this can be done in the Advanced LIGO projector as much as possible.

Thermal sensitivity of the CO_2 laser proved to be another significant source of trouble, causing the beam to wander and the output power to fluctuate. The Advanced LIGO projector design includes more active thermal management of the laser temperature, provision for stable, uninterrupted laser operation, and isolation of the laser's thermal environment from the rest of the projector, allowing scientists to work on the projector without disturbing the laser. These aspects of the design are discussed in Section 4.2.2.

Many interferometer operators have requested the capability to remotely align the TCS projector, due the frequent need to realign it during Enhanced LIGO commissioning. Remote steering of a 35W laser beam can present a safety hazard if not done correctly, but we think that a safe design is practical. The optical layout includes remotely steerable optics in two places: a pair of galvo mirrors between the beam shaping optics and the laser/AOM, and piezoactuators on the periscope mirror that directs the projector beam to the CP.

4.2.2 Dual temperature stabilized shuttered CO2 laser

The drift of the beam pointing has largely been traced to the Synrad 48-2 laser, whose output is very sensitive to its thermal state, likely due to flexure of the laser's optical resonator. It is essential that the laser be left on continuously when possible, and at a stable temperature. Work at LHO to stabilize the temperature of the CO_2 lasers by using the chillers to actuate on the temperature of the laser head has proved to be very successful in stabilizing the output power of the CO2 lasers, and drift has been reduced significantly.[9]

In Advanced LIGO, the laser will be enclosed in a lightproof box, which will be stabilized to within 0.05K of a setpoint slightly above room temperature. The beam will exit the box through a 1" diameter AR-coated ZnSe window. When beam is not needed, a shutter on the box will divert the beam to a water-cooled beam dump. This beam dump and the beam path to it will also be in a lightproof enclosure, but not part of the thermally stabilized laser enclosure. The shutter will be latched in the closed position by a hasp. This gives the laser Class 1 status, allowing it to be left on continuously with the beam contained, while the projector table is in a laser safe environment.

The laser temperature will be controlled by its chiller, which will be configured to stabilize the temperature of a thermistor on the laser head, rather than stabilize the temperature of the coolant reservoir in the chiller itself. Additionally, the CO_2 laser will have its own Thermoflex 1400 chiller. A separate chiller will be used to cool the other components of the CO_2 laser projector table (AOM, AOM driver, and beam dumps). These components collectively dissipate much less heat, are less thermally sensitive, and present a fluctuating heat load that would complicate the

[9] Cheryl Vorvick, LHO ilog entry, Tue May 26 17:17:42 2009 UTC.

laser chiller operation if they added to its line. Together they generate only ~75W of waste heat which can be removed with a much smaller chiller.

Given the efficiency expected for the CO_2 laser projector and the expected power needed in the TCS annulus beam, the laser used by the projector will be the 50W Synrad 48-5 CO_2 laser. This is discussed further in Section 4.2.12.

4.2.3 Intensity Stabilization System (ISS)

The ISS in Advanced LIGO will be the same as in eLIGO.[10] Briefly, an AOM deflects a small fraction (~5-10%) of the laser beam to a dump, and a photodetector monitors intensity fluctuations on a pickoff beam from the undeflected beam. Fluctuation error signals are amplified, filtered, and fed back to the AOM drive power to divert more or less of the beam as needed.

4.2.3.1 AOM

The baseline AOM is the IntraAction AGD406-B1 used in Initial and Enhanced LIGO. There is evidence[11] of variation in the beam pointing of the undeflected beam through the eLIGO TCS AOM when the AOM drive voltage is changed. Figure 4 shows this effect. Therefore, the AOM level should not be used to vary the ISS gain without then confirming the alignment of the optical layout. We may want to test a different AOM for Advanced LIGO, such as the Isomet LS600-1011. As noted, the optical layout reimages the AOM to the first axicon, rendering the system insensitive to this pointing shift to first order.

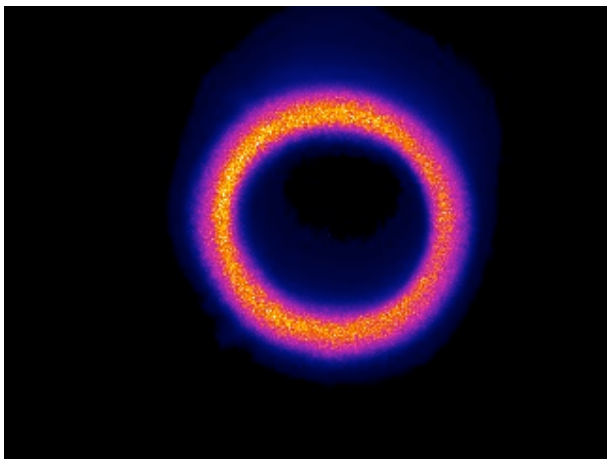

AOM at 1.1V

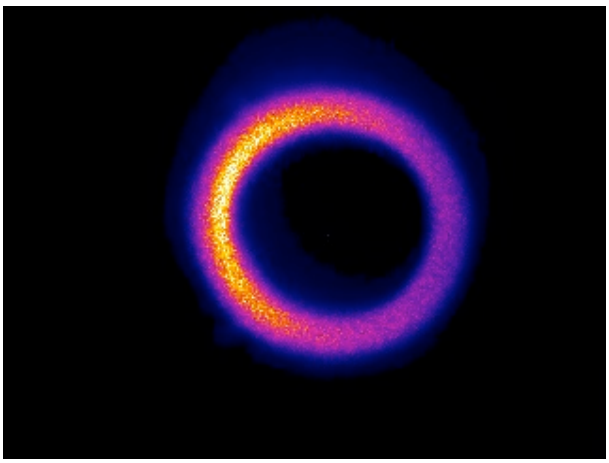

AOM at 3.0V

Figure 4: The annulus distribution at LHO for different AOM voltages. The slight blooming at the top of the image is due to convection on the paper beam target.

[10] "Enhanced LIGO TCS CO_2 Laser Intensity Servo Requirements," LIGO document T070224-01-D.

[11] LHO ilog: Wed 4 Mar 2009

4.2.3.2 In-loop and out-of-loop photodiodes

Advanced LIGO will use the same style of HgCdTe photodetectors used in Enhanced LIGO. These are Vigo PVM-10.6 PDs, which have a dark noise level <1nV/√Hz and a saturation voltage ~10mV, thus allowing ~10^{-7}/√Hz relative intensity noise.[12] Approximately 100-500 mW of light power is required on the PDs to reach this RIN level.

This type of PD tends to have spatially varying quantum efficiency across its active area. Thus, jitter noise will cause the laser beam to scan across these variations, which will create fluctuations in the PD output voltage. This design calls for these photodiodes to be placed at a conjugate plane of the waist of the CO_2 laser, where much of the high frequency jitter noise is likely to originate. Some jitter is also introduced by the AOM crystal, which is also at a conjugate plane to the ISS PDs.

4.2.3.3 ISS Electronics

The TCS ISS electronics will be the same as those in Enhanced LIGO,[13] with one modification: the TCS ISS Servo Board will include a test point to inject a signal into the AOM without breaking the servo loop, thus allowing simpler TCS→DARM transfer function measurement.

4.2.3.4 ISS Performance

We assume the spatial profile of heating on the CP shown in Figure 5. The intensity noise requirement for this CO_2 laser beam pattern incident on the CP has been studied.[14] We found that the noise coupling is dominated by thermoelastic and thermorefractive effects at the heated surface in the beam path, and not by flexure noise or elasto-optic effects. The required RIN is $3x10^{-7}$/√Hz,[15] achievable with TCS ISS at the Enhanced LIGO level.

4.2.4 Quad PD and Galvo Mirrors

The optical layout and projector components are designed to minimize the level of, and sensitivity to, beam pointing drift. Still, a monitor of the laser beam pointing is prudent. For this reason a Vigo PVMQ-10.6-1x1-SMA quad infrared PD will monitor the beam pointing through a pickoff after the laser and AOM, the two most drift-susceptible projector components. This PD is essentially the same design as the PVM-10.6 PDs used for ISS, but in a quadrant configuration with 1mm square elements.

Beam pointing drift detected by the quad PD can be corrected by the nearby pair of galvo mirrors. These galvos will be remotely steerable both from the control room during operation and locally at the table during projector alignment. Their travel will have hard limits to prevent the beam from

---

[12] see, for example, http://lhocds.ligo-wa.caltech.edu:8000/mLIGO/2008-03-16%3A_RIN_measurement

[13] "Low Noise Preamplifier," LIGO Document D070254; "TCS ISS Servo Board," LIGO Document D080351; "TCS AA Interface Board," LIGO Document D080315.

[14] "TCS Actuator Noise Coupling," LIGO document T060224-00-D.

[15] The requirement given in document T060224-00-D is $1x10^{-6}$/√Hz, but this assumes the higher-finesse cavities originally planned for Advanced LIGO. That document also assumes a 6.5 cm thick CP and 6.0 cm IFO beam waist, but these will not alter the noise requirements appreciably.

being steered into an unsafe location. These galvo mirrors are intended to have 1" diameter and slow operation (1 Hz BW). However, if smaller mirrors with sufficient bandwidth are available, they could potentially be used to suppress in-band jitter noise before it is sensed by the ISS PDs. They would then need to be moved from their current location in the optical layout to a position between the AOM and the ISS PD pickoff mirror. The requirements imposed by such a nested servo, especially upon the galvo bandwidth with respect to unity gain oscillations, have not yet been considered.

4.2.5 Mock Mach-Zehnder Beam Shaping Section

The Enhanced LIGO projector allows the operator to select either central heating or annular heating, but not both at the same time. It does this by using a pair of flipper mirrors to divert the laser beam around the axicons and through a central heating optics path. In addition to forcing a choice between the heating patterns, the central alignment is dependent upon the reproducibility of the flipper mirrors' positioning.

The Virgo TCS projector separates the two paths into a Mach-Zehnder configuration, with the power in the two paths independently adjustable. This has the advantage of allowing the test mass thermal state to remain constant during a loss of lock by leaving the annular heating alone and turning up the central heating power to make up for the loss of self-heating in the mirror. Interference between the two beam paths in the Mach-Zehnder cannot occur because the two heating patterns do not spatially overlap. Also, all beam paths travel only through fixed mirrors.

We adopt the Virgo scheme for the Advanced LIGO TCS projector, with the distinction that rather than using beamsplitters to separate and recombine the beams in the two arms, we use Brewster plate polarizers for the purpose, further ensuring that the two paths cannot interfere, and wasting less power at the recombination point. No other part of the layout is significantly affected by this choice. Note that the 'PBS' in Figure 2 implicitly includes a half-wave plate to adjust the beam polarization to direct the appropriate power to the two paths.

4.2.6 TCS Power Control and Sensing

Initial and Enhanced LIGO used single rotating polarizers to adjust the power of the TCS laser beam, which is linearly polarized when it exits the laser. Enhanced LIGO will use rotating half-wave plates followed by fixed polarizers for this purpose. The output beam will then more conveniently have a fixed polarization. A rotating polarizer followed by a fixed polarizer would adjust power more inexpensively; however, Brewster plate polarizers cause significant deviation and deflection of the transmitted beam, which then varies as the beam is rotated; compensating this in Enhanced LIGO required much work. In addition, certain rotation angles were discovered to backscatter power into one of the Enhanced LIGO TCS lasers. A rotating half-wave plate would mitigate these risks.

The power control will include a flipper-mounted shutter to switch off the beam power entirely. This shutter will use a mirror to divert the beam to a fixed beam dump.

Each arm of the Mach-Zehnder will have its own power control.

Some, but not all, of the Enhanced LIGO AOMs made the transmitted laser beam polarization elliptical, degrading the polarizer extinction ratio. Fixed polarizers will be placed after the AOMs to clean the polarization if necessary.

4.2.7 Beam Shaping Optics

4.2.7.1 Central Heating Path

The central heating path has historically been used for three purposes; to add heat to an underheated mirror, to maintain the thermal state of a mirror after an interferometer loses lock, and for alignment of the TCS projector onto the ITM. The first two functions use a beam of the same size and shape as the IFO science beam. The alignment function has been found to benefit from a smaller beam, which enables 'pinpoint' positioning of the heat source, which does not need to be Gaussian in profile. Advanced LIGO has a cold point design, and so should never be underheated, though static curvature errors may benefit from central heating at very low power operation. Advanced LIGO also has Hartmann sensors, which should allow measurement of the TCS beam pointing with very high accuracy during alignment. Therefore, only the thermal maintenance function of the central heating is anticipated for Advanced LIGO. This requires a Gaussian beam profile of the same size as the IFO science beam, which can be easily achieved with a telescope to convert the Gaussian beam size from the laser, and a fixed aperture to strip any sidelobes from the laser's output beam.

4.2.7.2 Annular Heating Path

Figure 5 shows a heating pattern on the CP that gives nearly ideal compensation of the ITM thermal aberrations,[16] in the case that the ITM ring heater is not operating. The total heat absorbed by the CP is 7.5 W. We assume hereafter that the CO_2 laser projector will deliver this spatial beam pattern, adjusted in some cases for non-normal incidence.

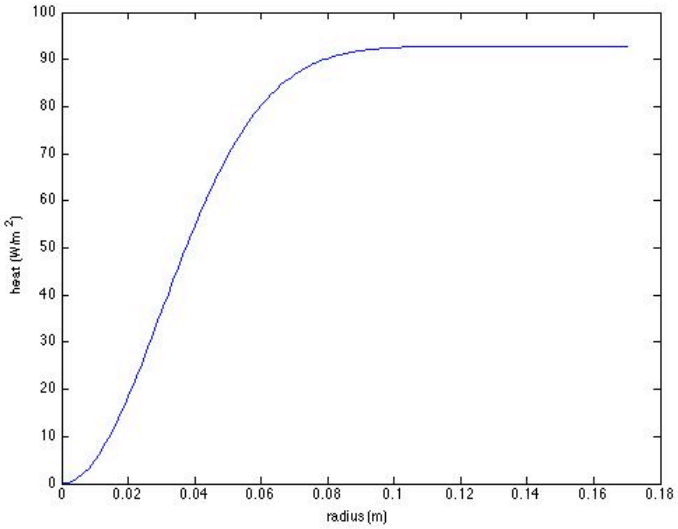

Figure 5: heat pattern on CP for nominal ITM absorption

[16] This pattern uses a simplified model that considers only thermorefractive and thermoelastic effects, and only coating absorption at the ITM HR surface with a 6cm spot size. The flats on the mirrors were not included in the model.

In general, the self-heating spatial pattern in the ITM at high power can have any number of ugly shapes, depending upon how inhomogeneous the absorption profile is. Generally, TCS will need to add more heat to the outside of the ITM, so we refer to the overheating compensation pattern as 'annular.'

The TCS projector continues the 'staring' design of Initial and Enhanced LIGO. The annular pattern is produced by fixed optics and cannot vary without replacing or repositioning those optics. There is currently no mature adaptive or scanning design that is not likely to inject noise into the interferometer GW channel.[17]

The design philosophy is to retain maximum flexibility in the annular beam shaping, within the constraint of the staring design. In practice, this means retaining the capability to put a variety of optics into the annular path to achieve the required spatial pattern. The Advanced LIGO projector design is therefore adopting several optical designs for this path, with the aim of selecting the best ones for the actual overheating patterns in Advanced LIGO as built.

The simplest design is a patterned mask, through which the laser beam is transmitted. This was the design used in Initial LIGO, where the mask pattern was drilled into a thin metal plate. This tends to be very inefficient, because the mask has its maximum transmission at its periphery, where the laser beam profile is least intense. The first Initial LIGO masks only transmitted ~30% of the light incident upon them. This may be sufficient, though, for Advanced LIGO.

Drilled masks also have the drawback that their transmittance is either 100% or 0%, and so any smooth variations in heating power must already be present on the illuminating laser beam. This is not a severe limitation, however. The CP has a thermal 'point spread function,' in that a point illumination will create a thermally broadened phase profile, so numerous small points of heating can produce a desired smooth heating pattern by varying the size or density of the points, or both. Furthermore, the mask can be appropriately defocused from the CP plane to smear out the sharp contrasts into a smoother pattern. Diffraction due to a limiting aperture past the mask can accomplish a similar effect. The 'gold star' mask used in some Initial LIGO TCS tables exploited this effect, at the cost of even lower efficiency, about 15%.

Finally, drilled transmissive masks generally need to block the center of the beam, while transmitting at the periphery. This raises the question as to how the center of the mask is supported.

The drilled mask has the advantages that it is inexpensive (sold by the dozen for a few hundred dollars), and easily designed and manufactured by a laser machining shop in a week.

There are slightly more complicated designs that answer the disadvantages of the drilled transmissive mask.

1) The drilled reflective mask. Here the desired spatial pattern is reflected from the mask, rather than transmitted through it. Since the negative of the transmissive hole pattern is used, there is no central region to support. The cost is that the surface of the mask now must be of optical quality, both in surface smoothness (easy for 10.6 micron radiation)

[17] "Auxiliary Optics Support System Conceptual Design Document, Vol. 1: Thermal Compensation System," LIGO document T060083-01-D, page 36.

and surface figure (also easy if the plate is reasonably thick. The Mach-Zehnder beam path would need to be folded to employ this scheme.

2) The drilled mask illuminated by axicons. In this case an axicon pair (as in Enhanced LIGO) efficiently converts the laser beam to rough annulus, and the mask strips away the unwanted parts. The mask could be either in front of or behind the axicons, although its transmittance pattern would depend upon this choice. This is essentially the design now used in Enhanced LIGO, but in a very rudimentary form: an input aperture strips the outer half of the beam before illuminating the first axicon. This makes Enhanced LIGO more robust to pointing errors rather than tailors the beam profile, but a more intricate aperture would accomplish both ends.

Which design is best will depend in part upon the compensation pattern required. We describe the baseline design here, which uses axicons followed by a mask. Figure 6 shows an axicon illumination pattern and mask transmittance that combined will produce the heating pattern shown in Figure 5. The axicons are of the same design as used in Enhanced LIGO, of 1" diameter and 3.4° cone angle, and are separated by 70 mm. The beam incident upon the first axicon has 4 mm spot size. Only the inner 4 mm radius of the beam leaving the second axicon is used (and shown in Figure 6), the mask blocking all light outside this radius. The mask would then be reimaged to the CP with 42.5x magnification by the projector. The efficiency of this beam shaping system is 55%.

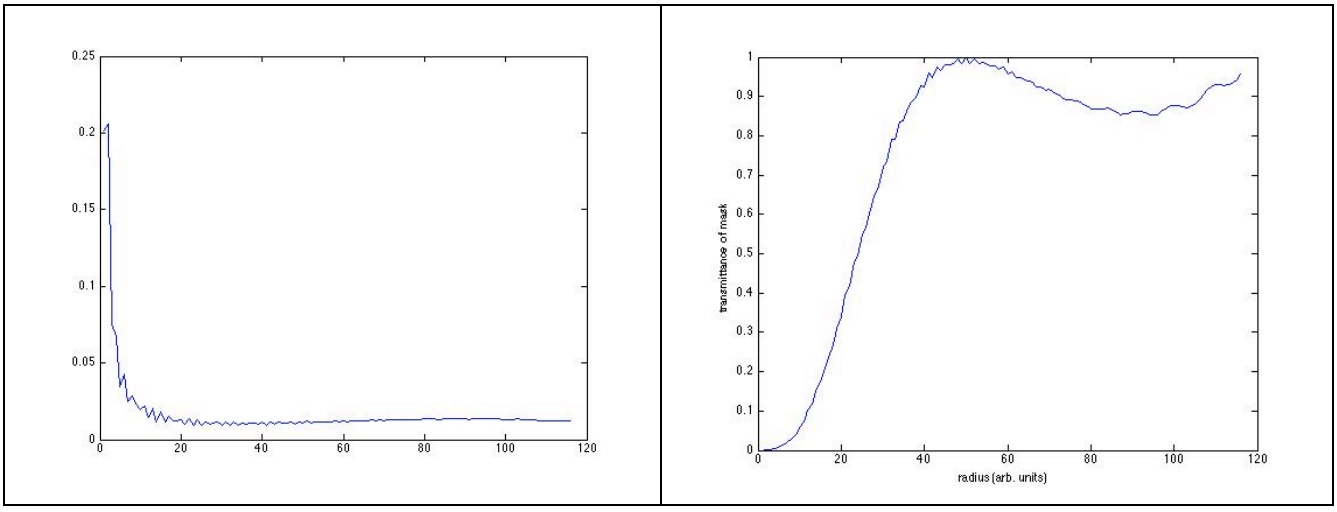

Figure 6: baseline annulus shaping optics. Left side; beam pattern after axicons. Right side; mask transmittance.

4.2.8 Power Monitor Photodetectors

These read the power delivered by the two paths, using pickoff mirrors to sample the beam. They are the same style of PD used in the ISS path. In the unlikely case that the operating TCS power is very low, the pickoff fraction may need to be so high that the PD will be damaged if the system goes to maximum power. If so, two PD's will be used in those paths, one optimized for high power, the other for low power, with a shutter blocking the low power PD unless the high power PD indicates a safe power level.

4.2.9 Annulus Monitor Camera

A fraction of the output of the mock Mach-Zehnder will be delivered to a paper target, the back side of which is viewed by a thermal imaging camera. This will provide verification that the pattern is correct, without the need to project the pattern across the LVEA floor, and readable from the control room. The paper target will be at an image plane of the CP face. The thermal imaging camera will be a Fluke Ti45HD.

4.2.10 Anamorphic Prism Pair (folded IFO only)

The TCS projector beam will illuminate the unfolded IFO's CPs at nearly normal incidence. The folded IFO TCS projector must illuminate the CP at a 45° angle due to the nearby folding mirror and elliptical baffle. To foreshorten the beam for delivery to these CPs, a ZnSe anamorphic prism pair will be used. These are available as custom parts from infrared optics vendors such as II-VI. To foreshorten the projection pattern appropriately for 45° angle of incidence on the CP, a wedge angle of 13.9° on each prism would be used.

4.2.11 In-vacuum Projection Optics

The CO_2 laser beam will enter the vacuum enclosure through ZnSe viewports of comparable design to those currently installed in Enhanced LIGO,[18] with protective ZnSe covers thermally interlocked to shut down the laser if contamination risks overheating the viewport.[19]

Unlike in initial and Enhanced LIGO, in-vacuum steering optics are needed to illuminate the CPs. These mirrors will be suspended, but only to reduce the weight of their support structure, not because they require seismic isolation. Figure 7 shows the locations of these mirrors for the unfolded IFOs. The beams appear to pass through the BS on their way to the CPs, but in fact pass under the BS. The suspensions for these mirrors will be similar in design to the suspension for the Elliptical Baffle beam dumps.

[18] "TCS Viewport Details," LIGO document E080448-00-V.

[19] "TCS ZnSe Viewport Protection Window Assembly," LIGO document D080617-v1.

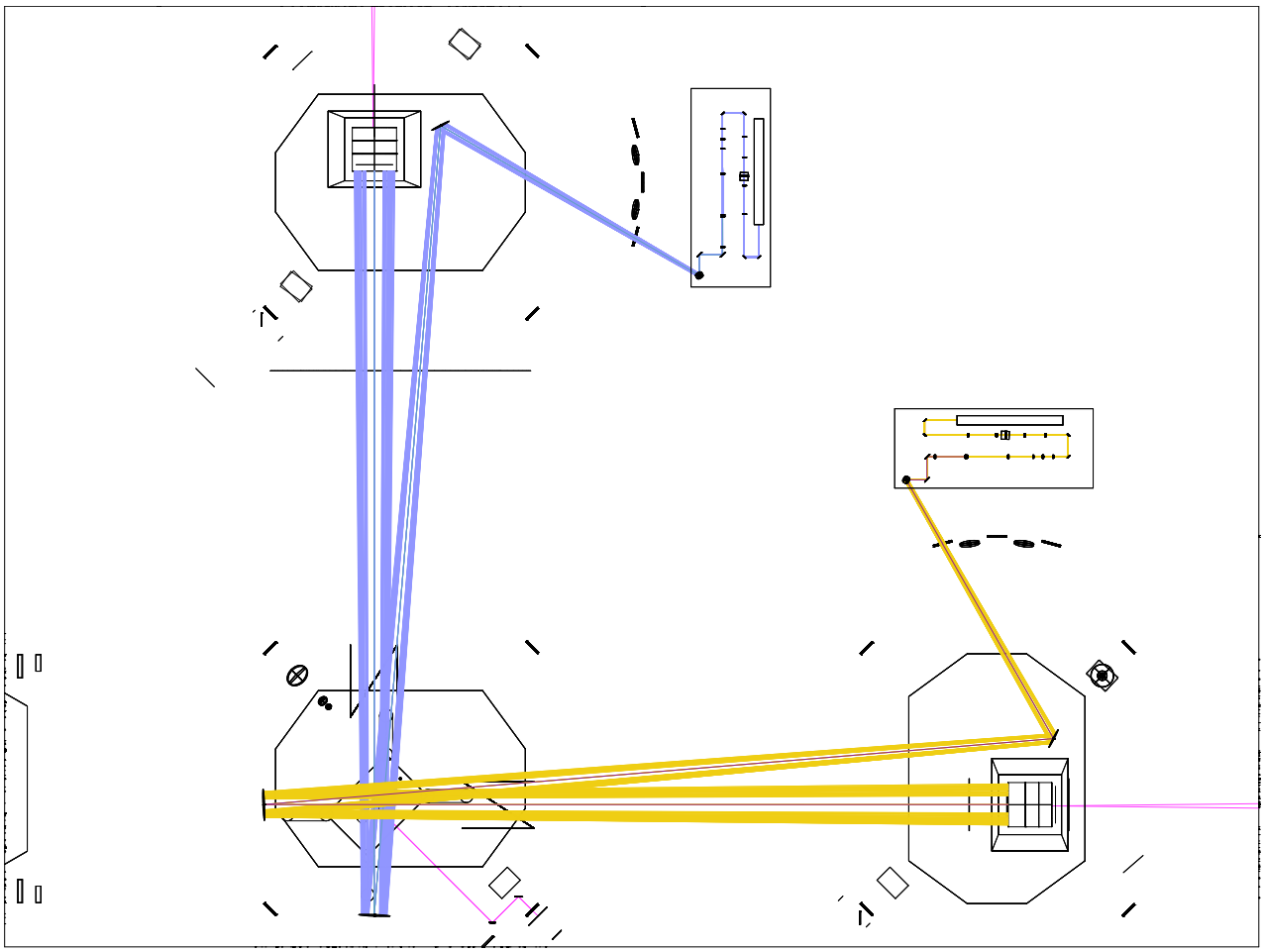

Figure 7: in-vacuum CO_2 laser projector optics for unfolded IFO.

Figure 8 shows the in-vacuum optics for the folded IFO. Note that in order to clear the Folding Mirror and Elliptical Baffle the CO_2 laser projector beam must be incident upon the CP at a 45° angle. At this angle of incidence, some fraction of the beam power will reflect from the CP and be at least partially intercepted by the Elliptical Baffle. The Elliptical Baffle should be made from black glass, rather than oxidized polished stainless steel, so that it absorbs this power rather than reflect it back to the CP. The portion of the reflected power not intercepted by the Elliptical Baffle may need to be intercepted by a secondary baffle in the position shown.

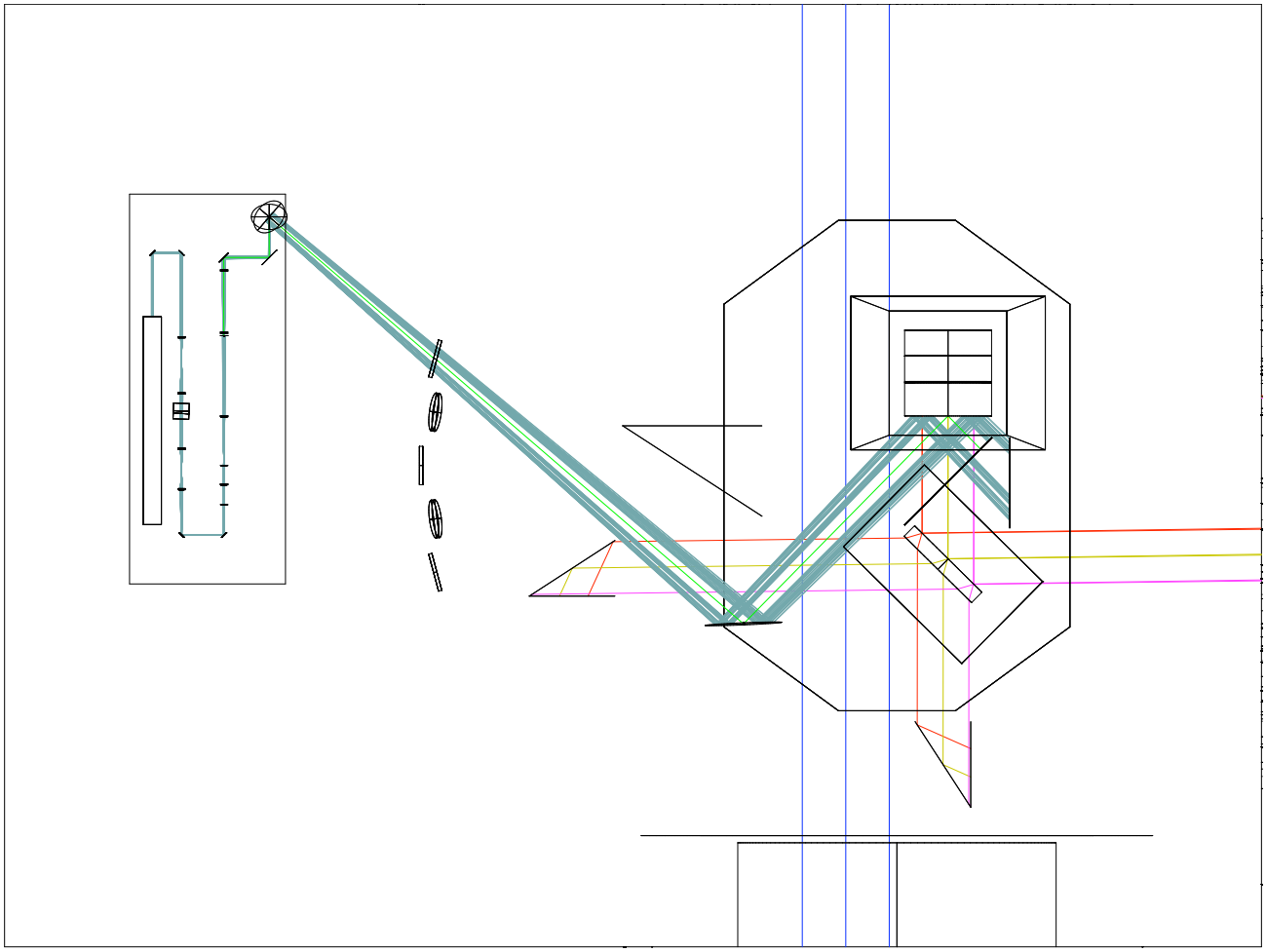

Figure 8: in-vacuum optics for folded IFO CO_2 laser projector.

All of the in-vacuum optics for the CO_2 laser projector are flat mirrors.

4.2.12 Projector Table Delivered Power

In the annular heating path, the transmission efficiencies of the various elements are given in Table 1.

Table 1: efficiency of carbon dioxide laser projector elements

Optical element & quantity	Transmittance	Reference
Laser enclosure window (1)	>98.5%	Meller Optics catalog
ZnSe lens (~6)	>98.5%	Meller Optics catalog
AOM (1)	>83%	Intraaction spec for insertion loss + 5% diffraction efficiency
Pickoff mirror (2)	95%	Directed Light, Inc. quote
Polarizer beam splitter (2)	98%	II-VI catalog

Central beam path (1)	1 W	Needed to provide central heating equal to self-heating of IFO
Power control (waveplate + polarizer) (1)	98% (polarizer)*98%(waveplate)	II-VI catalog
Mirror (~6)	>98%	Newport catalog
CP absorption	89%	Fused silica emissivity
Total	~49%	

The overall efficiency of 49% (not including the axicons) is comparable to that of the Enhanced LIGO projectors.

The amount of TCS power required for optimal compensation of 0.5 ppm absorption at full power is 7.5W; with the factor of two excess capacity specified in the Design Requirements, this rises to 15W. Assuming a 50W laser injected into the projector, there will be 24.5W of power available, and the annular beam shaping optics must therefore be 61% efficient. In practice, the Synrad 48-2 lasers in Enhanced LIGO have been providing more than 30W of power, despite a spec of only 25W. A 50W Synrad 48-5 laser would be just suitable for Advanced LIGO.

4.3 Hartmann Sensor

The purpose of Hartmann sensors in Advanced LIGO TCS is to continually measure the spatial profile of absorption-induced optical path distortion on transmission through each ITM and compensation plate arrangement and periodically measure the optical path distortion on transmission of each ETM. Each ITM therefore requires its own Hartmann sensor and probe beam. One “floating” Hartmann sensor is required per site for diagnostics on the ETMs.

4.3.1 Principle of Operation

Figure 9 shows how the Hartmann sensor measures changes in an optical wavefront.

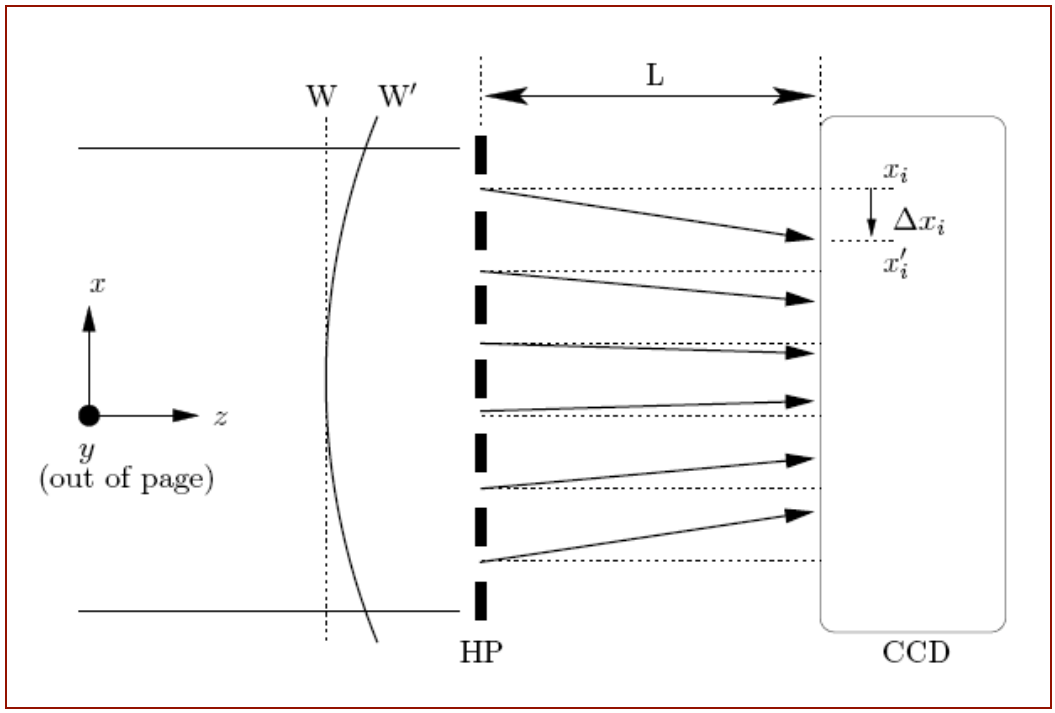

Figure 9: Illustration of Hartmann sensor operating principle.

A Hartmann sensor measures the change in the gradient of a wavefront relative to a reference wavefront. The gradient change is numerically integrated to give the wavefront change. The sensor consists of an opaque plate containing an array of apertures (a Hartmann plate) mounted a fixed distance in front of a CCD camera. A measurement is made as follows:

1) A reference wavefront W of a probe beam reflected from a cold mirror illuminates the Hartmann plate.
    a. A series of rays are formed. Each ray propagates *normal to the local gradient of the wavefront at its corresponding aperture.*
    b. The rays are incident on the CCD and produce an array of spots.
2) This reference spot array is stored as an image.
3) The 2D positions x_i of the spots are determined with sub-pixel accuracy using a centroiding algorithm.
    a. As a rough guide, the precision with which the centroid of a single spot can be resolved is the pixel diameter, D_p, (~12μm) divided by the square root of the number of electrons, N_e, in the most intense pixel in that spot (usually of the order of 200,000 electrons).
4) A thermal lens in the mirror changes the wavefront of the probe beam to W'.
    a. As the local gradient of the wavefront at each aperture changes, the propagation direction of the corresponding ray and spot position on the CCD changes.
    b. The spots move on the CCD to positions x_i'
    c. The change in the propagation direction of the ith ray, $\Delta\phi_i$, is given by $\Delta\phi_i = (x_i' - x_i)/ L$
5) The change in the propagation direction of the ray is equal to the change in the local gradient of the wavefront: $\Delta\phi_i = \nabla(W_i' - W_i) = \nabla(\Delta W_i)$.
6) This yields a discretized measurement of the gradient of the change of the wavefront, where

the change in the wavefront **is** the thermal lens.

7) The thermal lens can be found by numerically integrating this gradient measurement.

The performance of the Hartmann sensor has been investigated and demonstrated at the University of Adelaide.[20] Figure 10 shows an exploded view of the University of Adelaide Hartmann sensor. The 50 micron thick Hartmann plate is sandwiched between two aluminum blocks, each with a 36mm diameter hole in the center. This assembly is bolted to the front of a Dalsa 1M60 CCD camera. The window covering the CCD chip is removed to prevent stray reflections and interference effects.

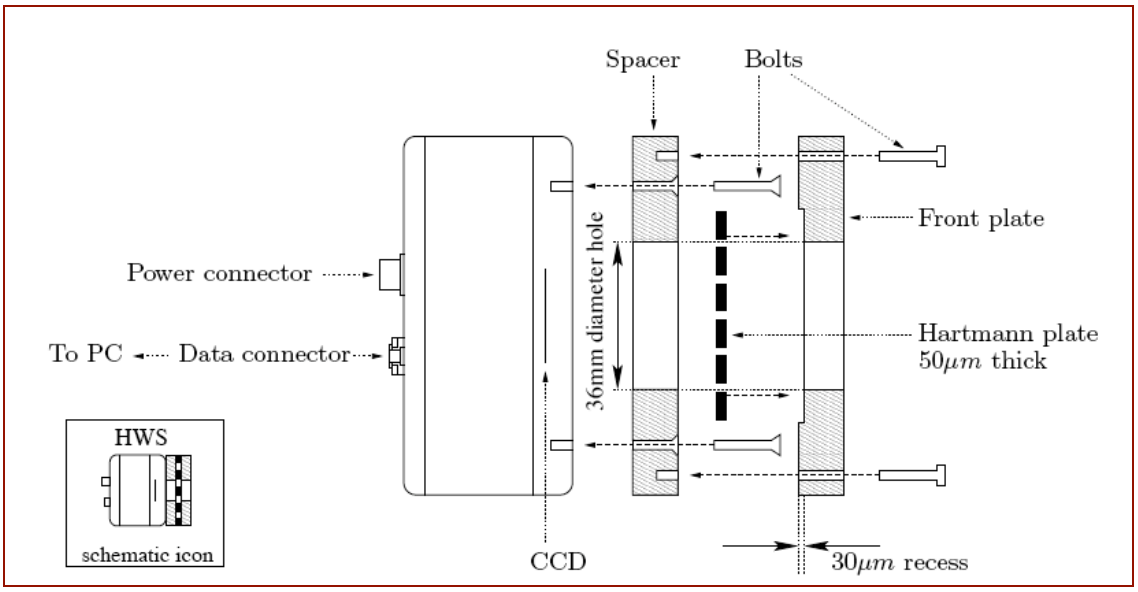

Figure 10: Exploded view of the University of Adelaide Hartmann sensor.

4.3.2 Thermal Drift in Hartmann Sensors

Hartmann sensors can be affected by thermal drift in components other than the optic under test. Some of these thermal drifts will cause true changes in the probe beam wavefront curvature, such as thermal defocus of delivery telescopes. Other drifts cause only apparent changes in the wavefront curvature, such as thermal expansion of the Hartmann plate. To measure and correct for these sorts of drifts, the Hartmann probe beams will include reference beam paths that are sensed by the same sensors and include much of the same delivery optics, but do not include the optics under test. These reference beam paths are described for the different core optics in Section 4.3.4 below.

[20] Brooks *et al*., "Ultra-sensitive wavefront measurement using a Hartmann sensor," Optics Express 15 (2007), pp. 10370-5; Brooks *et al.,* "Direct Measurement of Absorption-Induced Wavefront Distortion in High Optical Power Systems," Applied Optics 48 (2009) pp. 355-64.

4.3.3 List of Hartmann Sensors in Advanced LIGO

Table 2 lists the Hartmann sensor locations, probe wavelengths and optical layouts. The motivations for the probe wavelengths and optical layouts are given in Sections 4.3.4 and 4.3.5.3.

Table 2: Optical layouts of the Hartmann sensors

Location	Optic(s)	Wavelength	Optical Layout
L1- unfolded	ITMX+CP	980 nm[21]	2A
L1- unfolded	ITMY+CP	670 nm[22]	3A
L1- unfolded	ETMX	532 nm	1
L1- unfolded	ETMY	532 nm	1
H1- unfolded	ITMX+CP	980 nm	2A
H1- unfolded	ITMY+CP	670 nm	3A
H1- unfolded	ETMX	532 nm	1
H1- unfolded	ETMY	532 nm	1
H2- folded	ITMX+CP	670 nm	3B
H2- folded	ITMY+CP	980 nm	2B
H2- folded	ETMX	532 nm	1
H2- folded	ETMY	532 nm	1

4.3.4 Hartmann Sensor Optical Layouts

4.3.4.1 Hartmann Layout 1: ETM Sensors

The optics for the ETM Hartmann sensor are partially contained in the ETM Transmission Monitor, which is not yet fully designed. The ETM Transmon layout presented in **Figure 11** is incomplete but is nevertheless representative enough to show the essential features of the Hartmann sensor optical layout.

[21] This wavelength is provisional, and based upon the throughput analysis in section 4.3.5.3.

[22] This wavelength is provisional, and based upon the availability of a highly transmissive passband in the BS 50/50 coating at that wavelength.

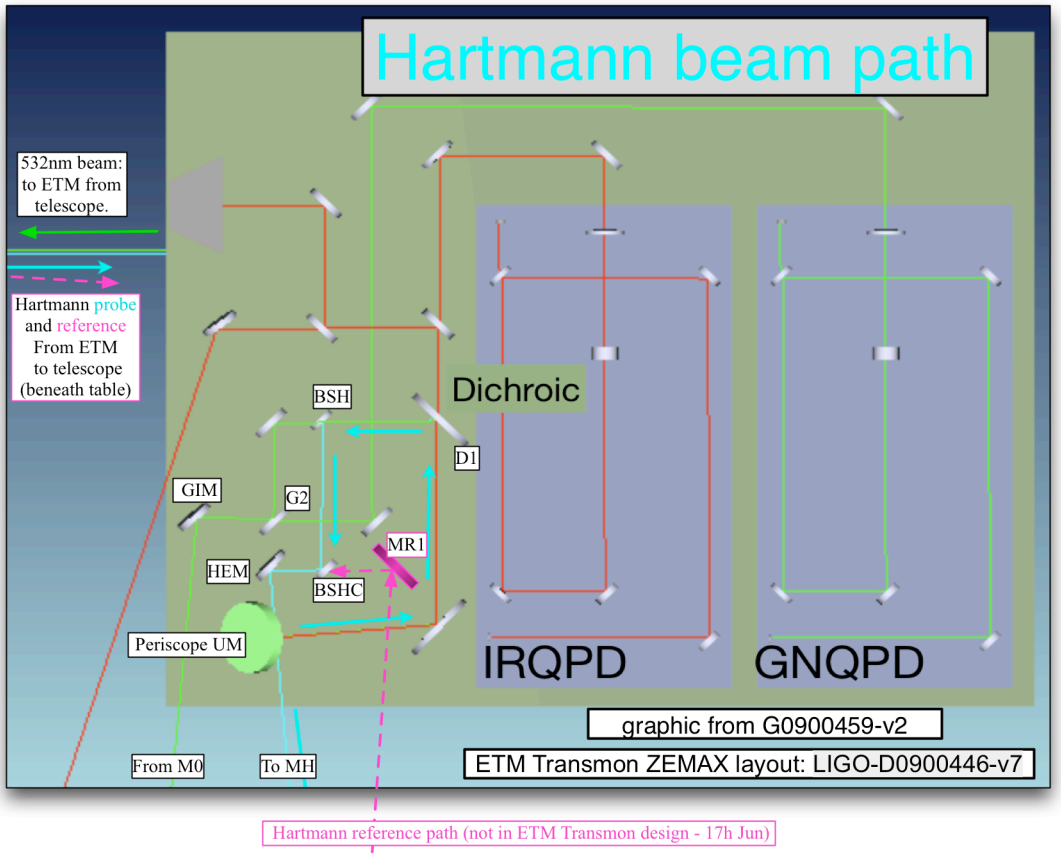

Figure 11: sample ETM Transmon table layout. Green (532nm) beam enters from M0 and propagates to ETM.

The ETM Hartmann sensor will use as its probe beam the 532 nm beam used by ISC for single-arm locking, as described in the ISC Preliminary Design Document.[23] The power of this beam will be about 10-50 mW. It is not anticipated that the Hartmann sensor and single-arm locking will ever operate simultaneously. However, if the 532 nm light resonates in the arm cavity during a Hartmann measurement it is likely to compromise the measurement. Therefore, the light will need to be slightly detuned during the Hartmann measurement, or the Hartmann measurement made immediately after breaking lock in the interferometer.

The Hartmann probe beam will reflect from the ETM HR face and pass through the ETM Transmon telescope, after which it reflects from G3 and BSH before transmission through the Beam Splitter Hartmann Combiner BSHC just below BSH in **Figure 11**.

The Hartmann reference probe beam is taken from the reflection of the ETM AR surface, passes through the ETM Transmon telescope off-axis, reflects from the mirror MR1, and recombines with the main Hartmann probe beam at BSHC. The main and reference Hartmann probe beams will be recombined with a slight angle between them.

[23] "AdvLIGO Interferometer Sensing and Control Preliminary Design," LIGO document T0900175-v1.

Figure 12 shows the layout of the Hartmann sensor optics outside the vacuum. A final telescope magnifies the probe beam to fit into the CCD array (magnification approximately 2x) and to reimage the ITM HR surface to the Hartmann sensor. A shutter at the focus of the telescope passes either the main or reference Hartmann probe beam, as desired. Finally, a bandpass filter blocks 1064nm light from reaching the CCD array.

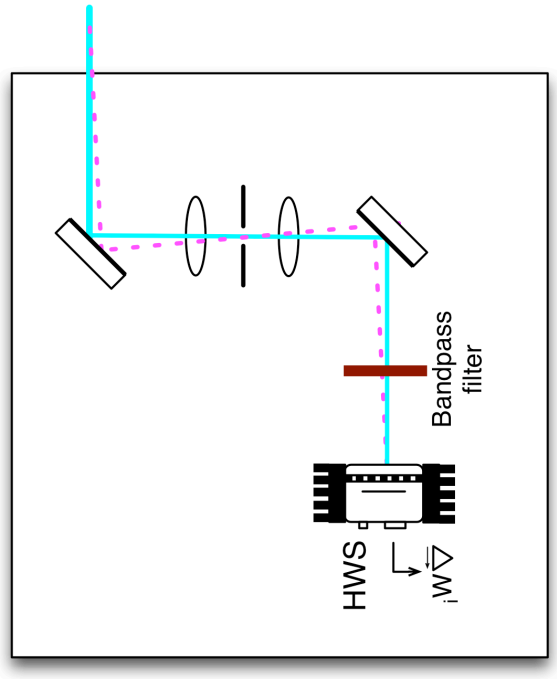

Figure 12: ETM Hartmann sensor optics outside vacuum.

The transmission of power through the optical system can be determined using Table 3 and Table 4 below.

Table 3: power budget for ETM Hartmann reference beam.

#	Description (transmitted through or reflected from)	Distance from previous (mm)	Beam Size (mm)	Optic Power (m^{-1})	Refl/Trans @ 532nm	Cumulative Trans.
1	Vacuum input window (M0) – trans.	?	2.0 mm	0 m^{-1}	T~0.995	0.995
2	Beamsplitter (G2) – refl.	?	2.0 mm	0 m^{-1}	R~0.5	0.497
3	Beamsplitter (G3) – refl.	?	2.0 mm	0 m^{-1}	R~0.5	0.249
4	Beamsplitter (D1) – trans.	?	2.0 mm	0 m^{-1}	T~0.5	0.125
5	ETM Telescope secondary – refl.	?	2.0 mm	??	R~0.995	0.125

6	ETM Telescope primary – refl.	?	40 mm	??	R~0.995	0.125
7	Reaction Mass (RM) AR surface 1 – trans.	?	40 mm	0 m^{-1}	T=0.999 [24]	0.12
8	Reaction Mass (RM) AR surface 2 – trans.	200 mm?	40 mm	0 m^{-1}	T=0.999 [25]	0.11
9	**End Test Mass (ETM) AR surface – refl.**	**5.0 mm?**	**40 mm**	**0 m^{-1}**	**R~0.01** [26] (0.001<R<0.02)	**1.1E-3**
10	Reaction Mass (RM) AR surface 2 – trans.	5.0 mm?	40 mm	0 m^{-1}	T=0.999	1.0E-3
11	Reaction Mass (RM) AR surface 1 – trans.	200 mm?	40 mm	0 m^{-1}	T=0.999	9.5E-4
12	ETM Telescope primary – refl.	?	40 mm	??	R~0.995	9.5E-4
13	ETM Telescope secondary – refl.	?	2.0 mm	??	R~0.995	9.5E-4
14	Hartmann PO (HPO) – refl.	?	2.0 mm	0 m^{-1}	R~0.995	9.5E-4
15	Hartmann beamsplitter (HBS) – refl.	?	2.0 mm	0 m^{-1}	R~0.5	4.8E-4
16	Vacuum exit window (MH) – trans.	?	2.0 mm	0 m^{-1}	T~0.995	4.8E-4
17	Hartmann turning mirror 1 (HTM1) – refl.	?	2.0 mm	0 m^{-1}	R~0.995	4.8E-4
18	Hartmann imaging lens 1 (HL1) – trans.	?	2.0 mm	4.0 m^{-1}	T~0.995	4.8E-4
19	Hartmann imaging lens 2 (HL2) – trans.	750 mm	4.0 mm	2.0 m^{-1}	T~0.995	4.8E-4
20	Hartmann turning mirror 2 (HTM2) – refl.	?	4.0 mm	0 m^{-1}	R~0.995	4.8E-4
21	Hartmann sensor	?	4.0 mm	-	-	4.8E-4

Table 4: power budget for ETM Hartmann main beam.

#	Description (transmitted through or reflected from)	Distance from previous (mm)	Beam Size (mm)	Optic Power (m^{-1})	Refl/Trans @ 532nm	Cumulative Trans.
1	Vacuum input window (M0) – trans.	?	2.0 mm	0 m^{-1}	T~0.995	0.995
2	Beamsplitter (G2) – refl.	?	2.0 mm	0 m^{-1}	R~0.5	0.497
3	Beamsplitter (G3) – refl.	?	2.0 mm	0 m^{-1}	R~0.5	0.249
4	Beamsplitter (D1) – trans.	?	2.0 mm	0 m^{-1}	T~0.5	0.125
5	ETM Telescope secondary – refl.	?	2.0 mm	??	R~0.995	0.125

[24] "Advanced LIGO End Reaction Mass Coating Specification," LIGO document E0900140.

[25] Ibid.

[26] "Advanced LIGO End Test Mass Coating Specification," LIGO document E0900068.

6	ETM Telescope primary – refl.	?	40 mm	??	R~0.995	0.125
7	Reaction Mass (RM) AR surface 1 – trans.	?	40 mm	0 m^{-1}	T=0.999	0.12
8	Reaction Mass (RM) AR surface 2 – trans.	200 mm?	40 mm	0 m^{-1}	T=0.999	0.11
9	End Test Mass (ETM) AR surface – trans.	5.0 mm?	40 mm	0 m^{-1}	T=0.99	0.10
10	End Test Mass (ETM) HR surface – refl.	200 mm	40 mm	1971 m^{-1}	R=0.95	0.10
11	End Test Mass (ETM) AR surface – trans.	200 mm	40 mm	0 m^{-1}	T=0.99	0.10
12	Reaction Mass (RM) AR surface 2 – trans.	5.0 mm?	40 mm	0 m^{-1}	T=0.999	1.0E-3
13	Reaction Mass (RM) AR surface 1 – trans.	200 mm?	40 mm	0 m^{-1}	T=0.999	9.5E-4
14	ETM Telescope primary – refl.	?	40 mm	??	R~0.995	9.5E-4
15	ETM Telescope secondary – refl.	?	2.0 mm	??	R~0.995	9.5E-4
16	Hartmann PO (HPO) – refl.	?	2.0 mm	0 m^{-1}	R~0.995	9.5E-4
17	Hartmann beamsplitter (HBS) – refl.	?	2.0 mm	0 m^{-1}	R~0.5	4.8E-4
18	Vacuum exit window (MH) – trans.	?	2.0 mm	0 m^{-1}	T~0.995	4.8E-4
19	Hartmann turning mirror 1 (HTM1) – refl.	?	2.0 mm	0 m^{-1}	R~0.995	4.8E-4
20	Hartmann imaging lens 1 (HL1) – trans.	?	2.0 mm	4.0 m^{-1}	T~0.995	4.8E-4
21	Hartmann imaging lens 2 (HL2) – trans.	750 mm	4.0 mm	2.0 m^{-1}	T~0.995	4.8E-4
22	Hartmann turning mirror 2 (HTM2) – refl.	?	4.0 mm	0 m^{-1}	R~0.995	4.8E-4
23	Hartmann sensor	?	4.0 mm	-	-	4.8E-4

4.3.4.2 Hartmann Layout 2: ITMY Folded and ITMX Unfolded

Figure 13 shows the optical layout of the unfolded ITMX Hartmann sensor, called 2A in Table 2; the folded ITMY layout is similar. The Hartmann probe beams follow much of the same path as the IFO POX beam. After injection from the Hartmann sensor table near HAM4, the beam is injected into the vacuum to a series of steering mirrors and telescopes that deliver the beam to a dichroic beamsplitter, where it is combined with the 1064 nm POX beam coming the other way. The beam is then reflected from a steering mirror next to SR2 to SR3, reflects from SR3 to the BS, and then reflects off the AR face of the beamsplitter to ITMX, reflects from ITMX, and then retraces its path out of the vacuum.

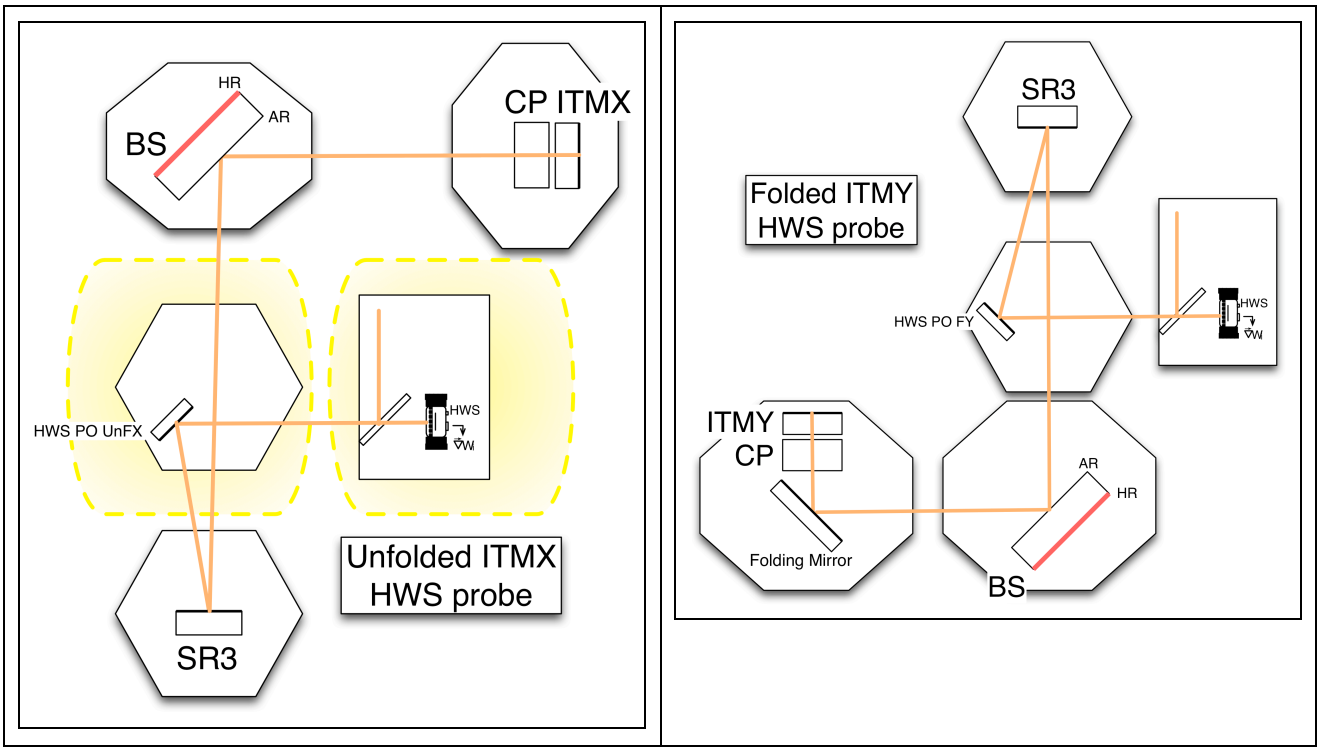

Figure 13: Left, optical layout 2A of unfolded ITMX Hartmann probe beam. Right, optical layout 2B of folded ITMY Hartmann probe beam. Highlighted areas are shown in detail in Figure 14.

Figure 14 shows in more detail the Hartmann sensor optical layout in HAM4 and on the table next to it. The optical layout was designed to image the ITM onto the Hartmann plate, to demagnify by 24x and to direct an approximately collimated onto the Hartmann sensor. The Hartmann probe beam must reflect from SR3 collimated and with 112mm radius. The telescope on HAM4 is designed to mode-match the beam from the Hartmann sensor table to SR3 in this manner before combination with the POX beam.

The Hartmann reference beam is picked off from the Hartmann probe beam using a dichroic beamsplitter that transmits 99% of the Hartmann probe wavelength (provisionally 980 nm) and transmits 100% of the 1064 nm beam. The transmitted 99% of the Hartmann beam travels to ITMX as described above. The reflected 1% is sent to SR3, reflected back to a reference mirror on HAM5, and then retraces its path back out of the vacuum. The probe beam is slightly misaligned upon reflection so that it can be separated from the Hartmann main beam outside the vacuum on the Hartmann sensor table in the same manner described for the ETM Hartmann sensor in Section 4.3.4.1.

Ideally, the BS AR surface should be 100% reflective for the Hartmann sensor probe beam wavelength. If this cannot be done, the Hartmann beam should be slightly misaligned from the IFO beam in order to prevent multiple bounce paths of the beam in the recycling cavities from reaching the sensor.

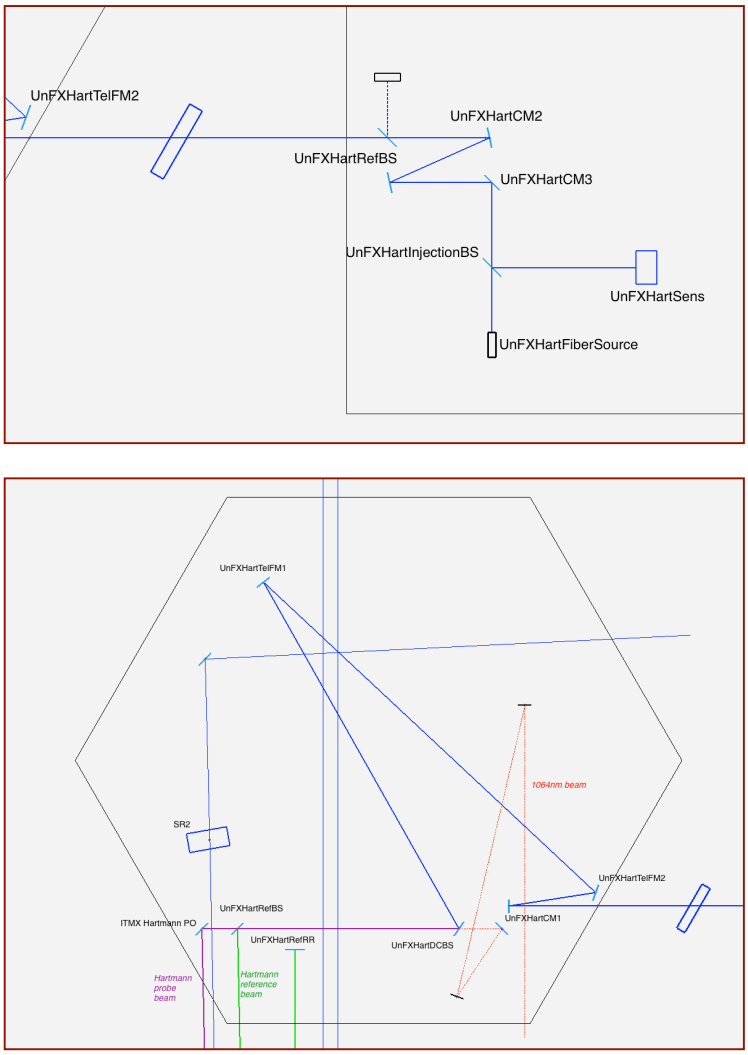

Figure 14: Top, Hartmann sensor source and input optics. Bottom, detail of Hartmann sensor layout 2 in HAM4. The Hartmann main beam is blue, POX is red, the two where they overlap is purple. The Hartmann reference beam is green.

Table 5 and Table 6 show the approximate distance between optics, the Hartmann beam size at these optics, the power of each optic (in m^{-1}) and an estimated power budget for the main and reference Hartmann probe beams for optical layout 2A.

An optical layout, Layout 2B, for HWS-Y in the folded IFO (HWS-Y-F) still needs to be designed. It is expected to be very similar to 2A, however, given the similarities in the two layouts.

Table 5: Optical path of unfolded ITMX Hartmann reference beam, in-vacuum.

#	Description - transmitted through or reflected from	Dist. from previous (mm)	Beam Size (mm)	Optic Power (m-1)	Refl/Trans @ 980 nm			Cumulative Trans.
1	Hartmann fiber source - (UnFXHartFiberSource)	-	8.23	-		1		1
2	Injection beamsplitter - (UnFXHartInjectionBS) -	345 mm	7.93	0 m-1	T~	0.5		5.0E-01
3	ITM imaging curved mirror 3 (UnFXHartCM3) - refl.	203 mm	7.76	2.5 m-1	R~	1		5.0E-01
4	Turning mirror 3 (UnFXHartTM3) - refl.	245 mm	1.95	0 m-1	R~	1		5.0E-01
5	ITM imaging curved mirror 2 (UnFXHartCM2) - refl.	262 mm	12.33	1.5625 m-1	R~	1		5.0E-01
6	On-table reference beamsplitter	250 mm	12.61	0 m-1	T~	0.99	*	5.0E-01
7	Vacuum input window -	520 mm	13.19	0 m-1	T~	1		5.0E-01
8	ITM imaging curved mirror 1 (UnFXHartCM1) - refl.	650 mm	13.91	0.25 m-1	R~	1		5.0E-01
9	Turning mirror 2 (UnFXHartTM2) - refl.	324 mm	12.01	0 m-1	R~	1		5.0E-01
10	Turning mirror 1 (UnFXHartTM1) - refl.	1675 mm	2.23	0 m-1	R~	1		5.0E-01
11	Dichroic beamsplitter (UnFXHartDCBS) - refl.	1466 mm	6.34	0 m-1	R~	0.95	?	4.7E-01
12	In-vacuum ref. beamsplitter (UnFXHartRefBS) - refl.	816 mm	11.11	0 m-1	R~	0.01	*	4.7E-03
13	Signal recycling mirror 3 (SR3) - refl.	15620 mm	101.36	2.94E-2 m-1	R~	0.991	?	4.7E-03
14	In-vacuum ref. retroreflector (UnFXHartRefRR) - refl.	15070 mm	99.55	0 m-1	R~	0.99		4.6E-03
15	Signal recycling mirror 3 (SR3) - refl.	15070 mm	96.75	2.94E-2 m-1	R~	0.991	?	4.6E-03
16	In-vacuum ref. beamsplitter (UnFXHartRefBS) - refl.	15620 mm	5.05	0 m-1	R~	0.01	*	4.6E-05
17	Dichroic beamsplitter (UnFXHartDCBS) - refl.	816 mm	0.27	0 m-1	R~	0.95	?	4.3E-05
18	Turning mirror 1 (UnFXHartTM1) - refl.	1466 mm	8.34	0 m-1	R~	1		4.3E-05
19	Turning mirror 2 (UnFXHartTM2) - refl.	1675 mm	18.04	0 m-1	R~	1		4.3E-05
20	ITM imaging curved mirror 1 (UnFXHartCM1) - refl.	324 mm	17.01	0.25 m-1	R~	1		4.3E-05
21	Vacuum input window -	650 mm	14.95	0 m-1	T~	1		4.3E-05
22	On-table reference beamsplitter -	520 mm	9.49	0 m-1	T~	0.99	*	4.3E-05
23	ITM imaging curved mirror 2 (UnFXHartCM2) - refl.	250 mm	1.92	1.5625 m-1	R~	1		4.3E-05
24	Turning mirror 3 (UnFXHartTM3) - refl.	262 mm	9.34	0 m-1	R~	1		4.3E-05
25	ITM imaging curved mirror 3 (UnFXHartCM3) - refl.	245 mm	8.84	2.5 m-1	R~	1		4.3E-05
26	Injection beamsplitter - (UnFXHartInjectionBS) - refl.	203 mm	8.43	0 m-1	R~	0.5		2.2E-05
27	Hartmann Wavefront Sensor (UnFXHartSens) - refl.	262 mm	7.9	0 m-1				2.2E-05

Table 6: Optical path of unfolded ITMX Hartmann main probe beam, in-vacuum.

#	Description - transmitted through or reflected from	Dist. from previous (mm)	Beam Size (mm)	Optic Power (m^{-1})	Refl/Trans @ 980 nm			Cumulative Trans.
1	Hartmann fiber source - (UnFXHartFiberSource)	-	8.23	-		1		1
2	Injection beamsplitter - (UnFXHartInjectionBS) -	345 mm	7.93	0 m^{-1}	T~	0.5		5.0E-01
3	ITM imaging curved mirror 3 (UnFXHartCM3) - refl.	203 mm	7.76	2.5 m^{-1}	R~	1		5.0E-01
4	Turning mirror 3 (UnFXHartTM3) - refl.	245 mm	1.95	0 m^{-1}	R~	1		5.0E-01
5	ITM imaging curved mirror 2 (UnFXHartCM2) - refl.	262 mm	12.33	1.5625 m^{-1}	R~	1		5.0E-01
6	On-table reference beamsplitter	250 mm	12.61	0 m^{-1}	T~	0.99	*	5.0E-01
7	Vacuum input window - trans.	520 mm	13.19	0 m^{-1}	T~	1		5.0E-01
8	ITM imaging curved mirror 1 (UnFXHartCM1) - refl.	650 mm	13.91	0.25 m^{-1}	R~	1		5.0E-01
9	Turning mirror 2 (UnFXHartTM2) - refl.	324 mm	12.01	0 m^{-1}	R~	1		5.0E-01
10	Turning mirror 1 (UnFXHartTM1) - refl.	1675 mm	2.23	0 m^{-1}	R~	1		5.0E-01
11	Dichroic beamsplitter (UnFXHartDCBS) - refl.	1466 mm	6.34	0 m^{-1}	R~	0.95	?	4.7E-01
12	In-vacuum ref. beamsplitter (UnFXHartRefBS) - trans.	816 mm	11.11	0 m^{-1}	T~	0.99	*	4.7E-01
13	Hartmann PO mirror (ITMX Hartmann PO) - refl.	131 mm	11.87	0 m^{-1}	R~	1		4.7E-01
14	Signal recycling mirror 3 (SR3) - refl.	15181 mm	100.57	2.94E-2 m^{-1}	R~	0.991	?	4.6E-01
15	Beamsplitter (BS) AR surface - refl.	19395 mm	99.16	0 m^{-1}	R~	0.011	?	5.1E-03
16	Compensation Plate AR surface 1 - trans.	4853 mm	98.81	0 m^{-1}	T~	0.953	?	4.8E-03
17	Compensation Plate AR surface 2 - trans.	130 mm	98.79	0 m^{-1}	T~	0.953	?	4.6E-03
18	ITMX AR surface - trans.	5 mm	98.79	0 m^{-1}	T~	0.953	?	4.4E-03
19	ITMX HR surface - refl.	10 mm	98.79	7.36E-4 m^{-1} (in air)	R~	0.991	?	4.4E-03
20	ITMX AR surface - trans.	10 mm	98.79	0 m^{-1}	T~	0.953	?	4.1E-03
21	Compensation Plate AR surface 2 - trans.	5 mm	98.79	0 m^{-1}	T~	0.953	?	4.0E-03
22	Compensation Plate AR surface 1 - trans.	130 mm	98.79	0 m^{-1}	T~	0.953	?	3.8E-03
23	Beamsplitter (BS) AR surface - refl.	4853 mm	98.78	0 m^{-1}	R~	0.011	?	4.1E-05
24	Signal recycling mirror 3 (SR3) - refl.	19395 mm	97.65	2.94E-2 m^{-1}	R~	0.991	?	4.1E-05
25	Hartmann PO mirror (ITMX Hartmann PO) - refl.	15181 mm	9.45	0 m^{-1}	R~	1		4.1E-05
26	In-vacuum ref. beamsplitter (UnFXHartRefBS) - trans.	131 mm	8.69	0 m^{-1}	T~	0.99	*	4.1E-05

27	Dichroic beamsplitter (UnFXHartDCBS) - refl.	816 mm	3.95	0 m^{-1}	R~	0.95 ?	3.9E-05
28	Turning mirror 1 (UnFXHartTM1) - refl.	1466 mm	4.57	0 m^{-1}	R~	1	3.9E-05
29	Turning mirror 2 (UnFXHartTM2) - refl.	1675 mm	14.3	0 m^{-1}	R~	1	3.9E-05
30	ITM imaging curved mirror 1 (UnFXHartCM1) - refl.	324 mm	14.8	0.25 m^{-1}	R~	1	3.9E-05
31	Vacuum input window - trans.	650 mm	13.66	0 m^{-1}	T~	1	3.9E-05
32	On-table reference beamsplitter	520 mm	12.75	0 m^{-1}	T~	0.99 *	3.8E-05
33	ITM imaging curved mirror 2 (UnFXHartCM2) - refl.	250 mm	5.08	1.5625 m^{-1}	R~	1	3.8E-05
34	Turning mirror 3 (UnFXHartTM3) - refl.	262 mm	5.72	0 m^{-1}	R~	1	3.8E-05
35	ITM imaging curved mirror 3 (UnFXHartCM3) - refl.	245 mm	8.25	2.5 m^{-1}	R~	1	3.8E-05
36	Injection beamsplitter - (UnFXHartInjectionBS) - refl.	203 mm	8.24	0 m^{-1}	T~	0.5	1.9E-05
37	Hartmann wavefront sensor	262 mm	8.23	0 m^{-1}			

Table 7 shows the calculations of the photon and photoelectron rates at the Hartmann sensor, and the camera frame rate for maximum sensitivity.

Table 7: Hartmann sensor camera frame rate calculations.

Transmission (probe and ref)	2×10^{-5}
Power transmitted (50mW input)	10^{-6} W
	5×10^{12} photons per second
Electrons per second on CCD (~ 5% Q.E.)	2.5×10^{11} electrons per second
Electrons per pixel on CCD	2.3×10^{5} electrons per pixel per second
Frames per second (~200,000 e- per saturated pixel)	1.15 frames per second
Attenuation required (for max 60 fps)	None

4.3.4.3 Hartmann Layout 3: ITMX Folded and ITMY Unfolded

The current design for the Hartmann sensor unfolded HWSY and folded HWSX probe beams use many of the existing core optics to inject the beam. This design is sub-optimal in its current form because it does not uniquely sample one ITM but rather returns a measurement of the average wavefront distortion of the two ITMs.

Figure 15 shows the optical layouts for the unfolded ITMY and folded ITMX probe beams. The probe beam is injected from the Hartmann sensor table outside the vacuum to steering mirrors and a telescope inside the HAM4 chamber, after which the Hartmann probe beam is combined with the 1064 nm beam leaking from the back of SR2. The Hartmann probe beam is then transmitted through SR2, where it joins the main IFO beam in the signal recycling cavity.

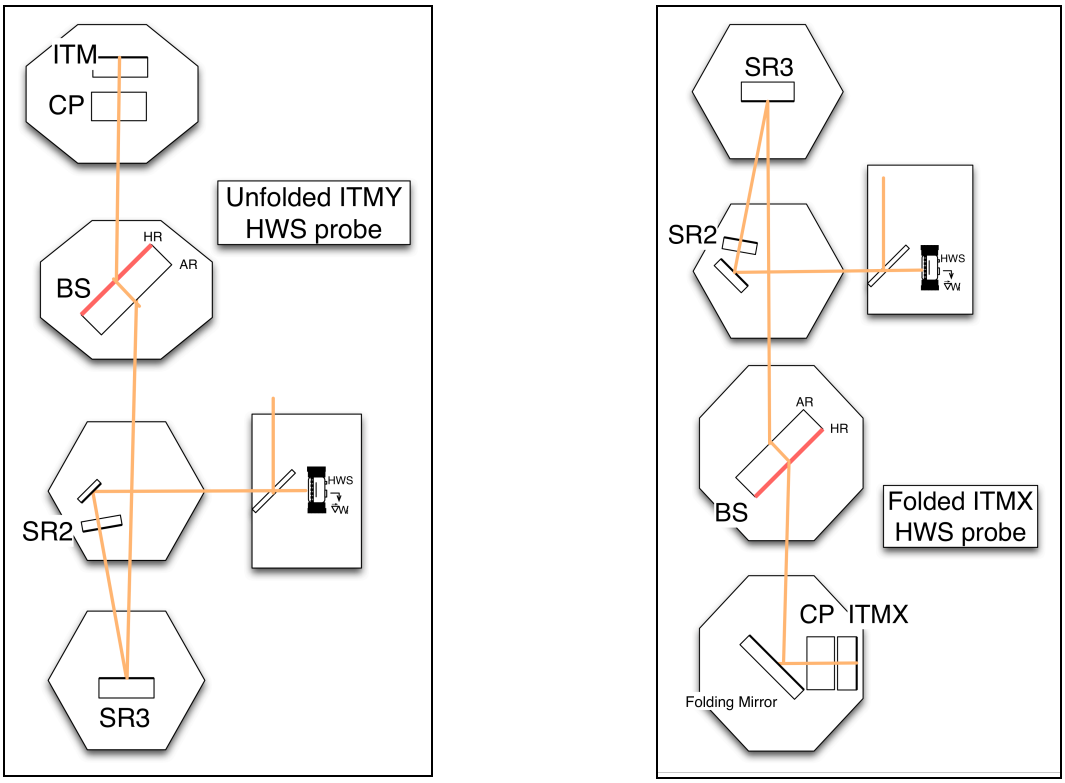

Figure 15: Optical layout of the unfolded ITMY (left, 2A) and folded ITMX (right, 2B) Hartmann probe beams.

The power budget for the unfolded ITMY Hartmann probe beam is given in Table 8, assuming 50% reflectivity for the BS 50/50 surface.

Table 8: power budget for unfolded ITMY Hartmann sensor probe beam.

#	Description - transmitted through or reflected from	Refl/Trans @ 980 nm	Cumulative Trans.
1	Hartmann fiber source	1	1.0E+00
2	Injection beamsplitter - trans.	T~ 0.5	5.0E-01
3	Signal recycling mirror 2 (SR2) – trans.	T~ 0.025	1.3E-02
4	Signal recycling mirror 3 (SR3) – refl.	R~ 0.99	1.2E-02
5	Beam splitter HR surface – trans.	T~ 0.5 ??	6.2E-03
6	ITMY HR - refl.	R~ 0.99	6.1E-03
7	Beam splitter HR surface – trans.	T~ 0.5 ??	3.1E-03
8	Signal recycling mirror 3 (SR3) – refl.	R~ 0.99	3.0E-03
9	Signal recycling mirror 2 (SR2) – trans.	T~ 0.025	7.6E-05
10	Injection beamsplitter - refl.	R~ 0.5	3.8E-05

If the BS 50/50 surface reflects 50% of the Hartmann probe light to ITMX, then the parasitic beam to this arm will have equal power to the desired probe beam and the Hartmann sensor will probe both mirrors equally, which is undesirable. The isolation of the ITMY from ITMX in the Hartmann sensor signal must rely upon very low reflectance of the BS 50/50 surface for the Hartmann probe beam wavelength. In the ideal case that the BS 50/50 reflectivity is zero, then the beam is completely decoupled from the ITMX arm and from the power recycling cavity. Figure 16 shows the general dependence of the relative power in the parasitic beam at the Hartmann sensor as a function of the BS 50/50 surface reflectivity. If, in addition, the transmittance of SR2 for the Hartmann probe light is 100%, then the Hartmann beam will not propagate to the SRM, and the probe beam will undergo an ideal single-pass reflection from ITMY. Although the Hartmann probe beam must reflect from SR3, it is not essential that the reflectivity be close to 100%.

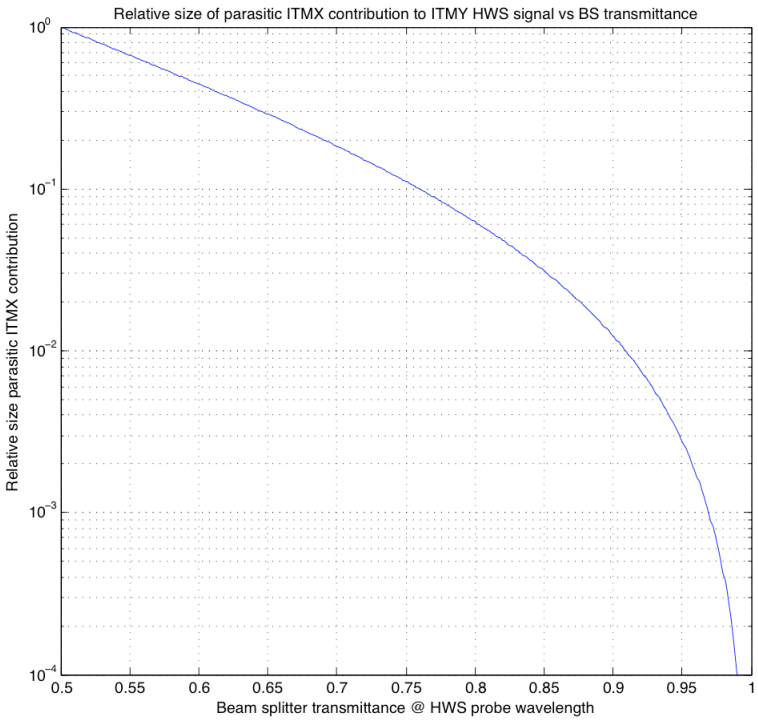

Figure 16: power in the parasitic ITMX probe beam relative to the power in the ITMY probe beam as a function of the BS transmittance at the HWS probe beam wavelength.

The final wavelength for these Hartmann sensors has not yet been identified. The 980 nm wavelength to be used for the other ITMs is probably too close to the IFO 1064 nm wavelength to easily permit the simultaneous 100% transmittances for the Hartmann probe beam, and 100% reflectance for SR2 and 50% reflectance for the BS at 1064 nm. A suitable combination of Hartmann probe wavelength and COC coating specifications must be identified. We note that the Hartmann probe beam polarization could be freely optimized in any such strategy.

The Hartmann reference wavefront would be produced similarly to that in Section 4.3.4.2.

4.3.5 Hartmann Sensor Hardware

The following section describes the hardware required for the Hartmann sensor system.

4.3.5.1 Camera

The camera used in the University of Adelaide prototype is a Dalsa 1M60, with the following specifications:

Feature	Unit	Spec
Product ID		DS-21-01M60
Total Data Rate	MHz	80
Max. Frame Rate	fr/sec	60
Pixel Size	μm	12 x 12
Resolution		1024 x 1024
Number of Camera Taps		2
Output Format		Base Camera Link
Sensitivity		12 bit

4.3.5.2 Hartmann Plate

The protoype Hartmann plate was a hexagonally-close-packed array of 150 μm diameter holes spaced 430 μm apart, laser drilled into a 50 μm thick brass plate to cover a 12.5x12.5 mm area. The laser drilling process positioned the holes to within ~1 μm.

The thermal expansion coefficient of brass is 20.3E-6 K^{-1}. As the Hartmann sensor's temperature changes the plate will expand and contract. The result of this is an apparent temperature-dependent quadratic defocus of the measured wavefront.[27]

The desired precision for the HWS is better than 1.3nm. Therefore, any temperature dependent defocus should appear to be less than this. This can be characterized in a number of ways. The strictest characterization states that across the diameter of the measured wavefront there should be less than 1.3nm distortion due to thermal effects. With a quadratic defocus that is roughly centered in a wavefront approximately 6 mm in diameter this equates to approximately 0.04K.

To ameliorate this problem passive and active thermal control strategies are being investigated at the University of Adelaide. The passive strategy consists of using a laser drilled invar sheet that has a substantially lower coefficient for thermal expansion. The active strategy involves using a thermistor as a sensor and a thermo-electric cooler as an actuator in a servo loop. Additionally any temperature dependent defocus could be characterized with additional temperature sensors within the vacuum and subtracted from the measured distortion.

[27] Aidan Brooks, "Hartmann Wavefront Sensors for Advanced Gravitational Wave Interferometers," Ph.D. thesis, University of Adelaide (2007).

4.3.5.3 Probe Beam Sources

The ETM Hartmann probe beam will be provided by ISC and is outside the scope of this document.

The ETM Hartmann probe beam will be coherent by virtue of its primary use to lock the arm cavity. Incoherent sources are generally preferable. The use of an incoherent/broadband source can improve the precision with which the centroids of the spots in the Hartmann pattern can be located by reducing cross-talk between adjacent spots by approximately 50%.[28] Additionally this eliminates the accumulation of interference fringes on the probe wavefront, which can substantially reduce the precision of the wavefront sensor.

Fiber-coupled sources are also preferable, as they would make it substantially easier to replace a source in the event that one failed, as potentially no re-alignment would be required.

The major problem in choosing a source is to pick one that can deliver enough photons to the Hartmann sensor to be effective. Since the probe beam is collinear (or nearly so) with the cavity beam the wavelength of the probe beam must differ enough so that the two beams can be separated. This is most problematic for the beams that probe the ITMs in power recycling cavity.

Figure 17 shows a variety of fiber-coupled sources available from QPhotonics, plotted as wavelength vs. power. The average frame rate of the AdvLIGO Hartmann sensors for each of these sources can be determined by calculating the percentage transmission through the particular optical train at each wavelength, multiplying by the power and multiplying by the appropriate quantum efficiency of the CCD, dividing by the number of pixels and the maximum number of electrons per pixel per frame.

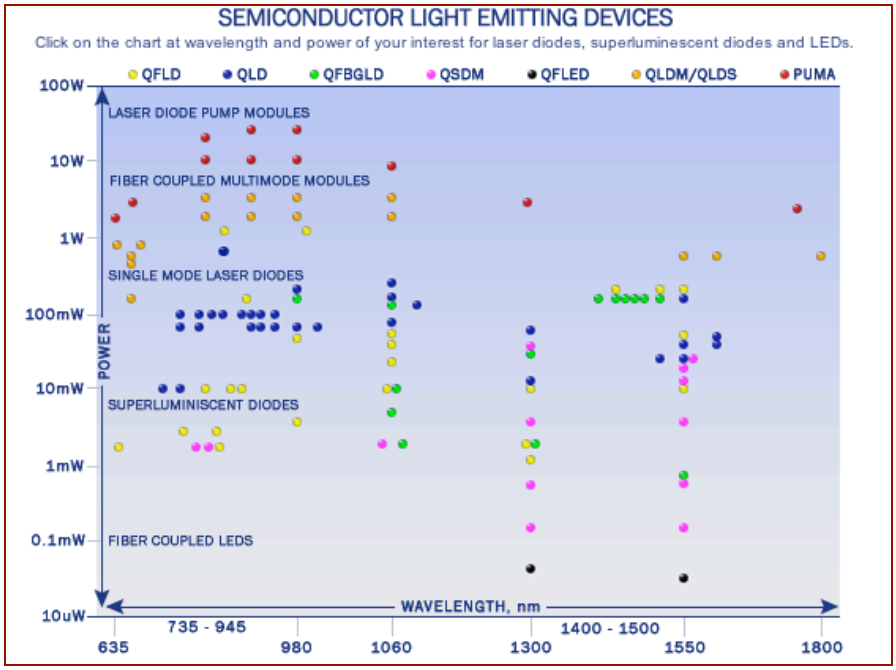

Figure 17: Fiber-coupled light sources available from QPhotonics.

[28] Ibid.

Some of the sources are capable of being tuned over a relatively wide range of wavelengths (~30nm). This is potentially very useful given that the transmission through the system fluctuates wildly with wavelength. Figure 18 illustrates this issue.[29] Any coating optimized for some performance at 1064 nm will have ripples in the visible portion of the spectrum, and the effective double-pass transmittance spectrum through several such optics will be the product of many such ripples. Unless a reasonable set of collective requirements on these coatings for some specific wavelength can be set, the precise wavelength where transmittance is best will not be predictable. Figure 18 shows that 30 nm tuning around a central wavelength within 650-750 nm would be adequate to sample a peak in the transmittance spectrum.

The data in Figure 18 can also be used to determine what frame rate can be achieved using a source of a given power, at a given wavelength. Figure 19 combines the information in Figure 17 and Figure 18 to show the power available from the QPhotonix sources, along with the power necessary at that wavelength to allow one frame-per-second (fps) sampling by the Hartmann sensor. The blue and green curves represent the power needed for one fps in TCSX and TCSY, respectively. The data show that there are several sources of suitable power from this vendor.

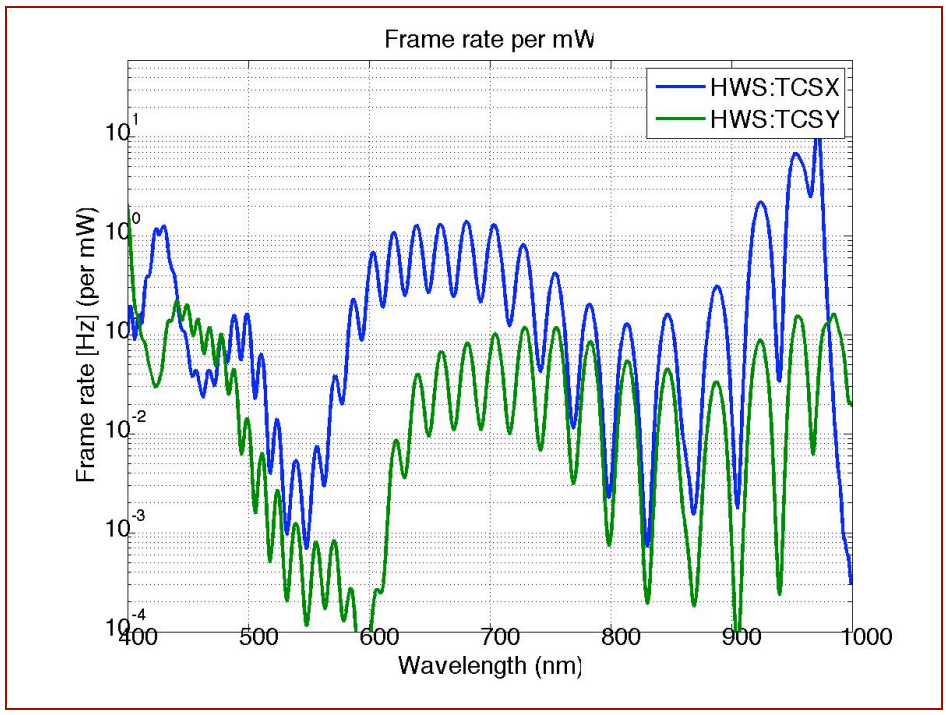

Figure 18: frame rate per mW of probe beam source, using representative AdLIGO mirror coating spectra.

It is worth pointing out that there are many vendors of visible and NIR, fiber pigtailed light sources besides QPhotonix, and that the transmittance curves here are *representative* of what the core optics will produce, and not specifications or requirements on core optic coating performance.

[29] Using data for AdLIGO test coatings provided by Laurent Pinard, LMA, private communication.

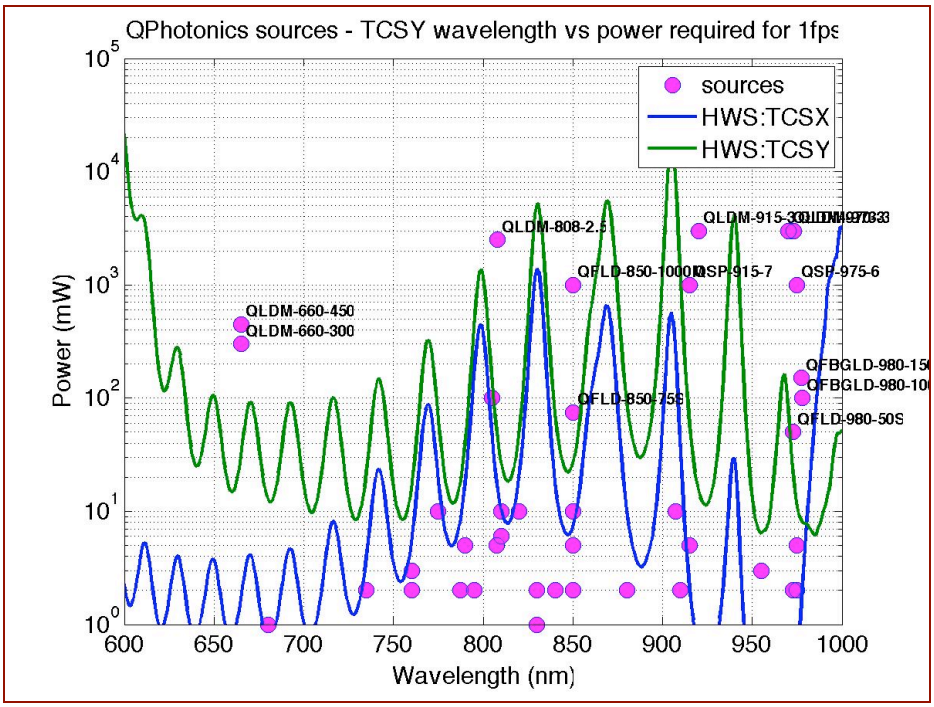

Figure 19: Comparison of QPhotonics source powers with power needed for 1 fps Hartmann sensor camera rate.

4.4 Twin-beam Optical Lever Sensor

The primary function of the shielded ring heater is to control the test mass's radii of curvature, which in turn determine the arm cavity mode structure. It is important therefore to monitor these radii of curvature.

This could in principle be done with the Hartmann sensors, but in practice would be difficult. The Hartmann sensors view the test masses through the AR faces, and so see a thermal lens in the substrate that is 16x larger than the thermal expansion which would need to be corrected. More difficult still is the case of the ITM, where the Hartmann sensor will also see the thermal lensing of the CO_2 laser projector, which will by design be making the thermoelastic deformation invisible from the recycling cavity. Separate monitors are needed to specifically monitor the HR radii of curvature.

The HR radii of curvature do not need to be monitored with the same high resolution as the ITM/CP thermal aberrations. Characterization in terms of a scalar radius of curvature is adequate. In the Conceptual Design Document, the resolution of the curvature measurement is given by the desire for a S/N of 10 for a double-pass measurement to be $\lambda/64$ for a 635 nm probe wavelength, much lower resolution than needed in the ITM/CP pair.

The TM radii of curvature will be monitored by the Optical Levers, which will use two beams rather than one as in initial LIGO. One beam will reflect from the center of the TM HR face and be sensitive only to the mirror tilt. The second beam will reflect 60 mm from the center of the TM HR face and be sensitive to both mirror tilt and HR ROC change. The differential motion of the two reflected spots measures the ROM change only.

The off-center beam will undergo a tilt of ~1 microradian due to thermal ROC change at full interferometer power if the shielded ring heaters are not used. The Optical Levers will measure tilt with better than this sensitivity, and since their sensitivity appears to be limited by flexure of the optical lever piers and the floor under them, differential measurements should be still more sensitive, and adequate to the purpose.

The detailed Optical Lever design will be found in the Optical Lever Design Documents.[30]

4.5 Bull's-eye Sensor

The Hartmann sensor provides a powerful diagnostic of the thermal lenses in individual mirrors of the interferometer. However, the fundamental figure of merit for the quality of the thermal compensation is the spatial mode structure of the interferometer beam itself. The bull's-eye sensor provides a simple diagnostic of the overlap of the RF sidebands with the carrier light.

When correctly installed, bull's-eye sensor measures the amplitude of the LG_{10} mode in the RF sideband fields of the power recycling cavity, in the Laguerre-Gauss basis where the carrier field is in the LG_{00} mode. For small variations of the RF sideband waist size and location relative to the carrier, these are the leading terms in the modal expansion of the RF field. Full derivations of the bull's-eye sensor signal are available elsewhere.[31] Originally developed for characterization of mode-matching into optical cavities, Stefan Ballmer adapted the sensor for use in servo control of TCS in initial LIGO.[32] We do not anticipate that the bull's-eye sensor will be used in a closed loop for TCS control in Advanced LIGO, but only for diagnostic purposes during commissioning.

In Advanced LIGO, there will be two pairs of RF sidebands, circulating within the coupled power and signal recycling cavities. These RF frequencies (9 and 45 MHz) are different from the 24 MHz used in initial LIGO. However, the bull's-eye sensor uses the same electronics as the WFS detectors, which are being adapted to Advanced LIGO radio frequencies, and these frequencies are well within the bandwidth of the photodiode. The same photodiodes will be used as in initial LIGO

The bull's-eye sensor will use either the POX beam or REFL beam to sample the recycling cavity fields. In either case, the bull's-eye sensor will reside on an optical table outside the vacuum with a telescope to produce a beam with the appropriate waist size and Gouy phase.

5 Phase Camera

The phase camera allows for a fuller resolution will allow for full characterization of the structure of the various optical fields at pickoff points of the interferometer where thermal lensing effects are visible: REFL, ASP, and POX.

---

[30] In progress.

[31] "Input Optics Final Design," R. Adhikari *et al.,* LIGO document LIGO T980009-01-D, section 9.3; "Determination and optimization of mode matching into optical cavities by heterodyne detection," G. Mueller *et al.,* Optics Letters 25 (2000), pp. 266-8.

[32] "LIGO interferometer operating at design sensitivity with application to gravitational radiometry," Stefan Ballmer, Ph.D thesis, MIT, 2006, section 2.8.4.

The design for the phase camera will be nearly identical to the design used in initial LIGO[33]. The primary difference will be to change the demodulation to the RF sideband frequencies used in Advanced LIGO. A reference optical field will be picked off from the pre-stabilized laser, frequency-shifted with an AOM, and coupled into a singlemode optical fiber for delivery to the appropriate ISCT, recoupling into free space, combination with the interferometer pickoff beam, and sensing with the phase camera. The precise location of this pickoff from the PSL is currently under discussion with the PSL and IO design teams.

An advanced phase camera design is currently being studied, using a fast, shuttered CCD camera to collect the demodulated light fields rather than scanning galvos and an RF PD. Such a design would readily be accommodated into Advanced LIGO as a future upgrade.

6 General TCS Procedures

6.1 Installation and Commissioning

6.1.1 Shielded Ring Heater

The shielded ring heater must be installed into the quad SUS structure before the installation of the test mass, with the two halves separated to the limits of the mounting slots to allow for the test mass positioning and welding. No installation tooling is required.

6.1.2 CO_2 Laser Projector

The in-vacuum optics and ZnSe windows will be installed into the vacuum envelope and aligned to the CPs using an aiming laser on the projector table after the core optics have been installed and aligned.

The CO_2 laser projector tables will be laid out on the LVEA at their final installed locations. The projected beam to the CPs will be coarsely aligned using a visible aiming laser, then more precisely aligned to the CP (and to its thermal lens) using the Hartmann sensor to monitor the resulting thermal phase profile.

6.1.3 Hartmann Sensor

The Hartmann sensor in-vacuum optics will be laid out and aligned after the core optics have been installed and aligned. Alignment of the Hartmann probe beams from the source to the CP and back out of the vacuum will be done during the in-vacuum optics installation. Alignment and imaging of the CP face to the Hartmann camera will be done by positioning a cruciform mask in front of the CP and focusing and centering the image at the Hartmann camera with the hole plate removed, and with the camera moved forward to the hole plate location.

[33] K. Goda *et al.,* "Frequency Resolving Spatiotemporal Wavefront Sensor," Optics Letters **29**, pp.1452-1454 (2004)

6.1.4 Twin-beam Optical Lever Sensor

The installation and commissioning of the optical lever sensor will be discussed in the design documentation for that subsystem.

6.1.5 Bull's-eye Sensor

The bull's-eye sensor resides outside the vacuum system and can be installed and commissioned after the ISC beams are made available on tables outside the vacuum.

6.1.6 Phase Camera

The phase camera resides outside the vacuum system and can be installed and commissioned after the ISC beams are made available on tables outside the vacuum. The PSL pickoff beam optics would ideally be installed during the PSL installation.